uc3m | Universidad Carlos III de Madrid

Aerospace Engineering

2017 - 2018

Bachelor Thesis

"Study of Magnetically Confined Plasma Dynamics with Cellular Automata"

Cristina Midori Fukuda León

Tutor

Luis Raúl Sánchez Fernández

September 2018. EPS Leganés, Madrid.

PREFACE

A star is being built on Earth. More than ever before, space is an inspiration for science. ITER, the most ambitious scientific project in history, is a worldwide collaboration inspired by the fusion processes taking place in the Sun. The Sun itself has become the model for a new source of clean, safe and virtually unlimited energy, fusion energy.

When it came to decide a topic for my final thesis, fusion energy appeared as a beautiful and promising field. Fusion energy is still not reliable at an industrial scale, and given the future global benefits it will provide, I could not overlook the obstacles that exists at present to achieve this goal. The research, results and conclusions presented in this thesis are intended to be a step further towards revealing the secrets to tenable nuclear fusion energy. For this, I had the great fortune to be advised by Dr. Raúl Sánchez, an expert in the field, whose good will to be my tutor was determinant to start this venture, and whose guidance was determinant to accomplish my goals.

This thesis has a fundamental and abstract perspective, pointing out at the essential causes that produce changes in transport in confined fusion plasma. Yet this abstraction is backed up by very real engineering developments in the world, being the ITER project the most important of them all.

Although the project has been done in the context of fusion plasma dynamics, the outcome is in fact a cellular automata, an abstract model of reality that could perhaps be employed in the future to explain some dilemma in aerospace plasma engines. However, it must be said that fusion plasmas and plasmas used in aerospace engines are radically different and separated from each other by millions of temperature degrees. An actual example of the connection of aerospace and fusion energy industries is the VASIMR rocket, that incorporates to plasma propulsion systems results obtained from research on heating methods for fusion plasma.

Energy affects everything, and in this context the most promising energy source for the future will surely draw the attention of the aerospace industry, even though its application is not immediate.

I very much hope that the reader may obtain as much pleasure and interest on reading this work as I got by doing it.

ABSTRACT

Nuclear fusion has many chances to become the primary energy source of the future. The great energy density of fusion reactions, together with the environmental and safety benefits that it encloses makes it a powerful alternative to existing energy sources and a smart response to the increase in energy demand.

Up to now, research has designated tokamaks as the best alternative to obtain fusion energy. However, their reliability has not yet been proved. To this matter, ITER, the most ambitious energy project in human history, is being built to demonstrate the viability of fusion energy by producing net positive energy in a giant tokamak.

Fusion plasmas inside Tokamaks are known to be turbulent. The instabilities created in the plasma by the great gradients they are subjected to, turn the issue of their confinement into a difficult goal to achieve. Part of the plasma escapes from the confinement volume, reducing the density in its core and decreasing the efficiency of the fusion reaction as well as the energy obtained from it. As a consequence, the net fusion energy produced may not be sustainable. More energy is used in the process than the one that is extracted from it. If fusion reactors are meant to be a reliable source of energy in the future, effective solutions to mitigate the effects of turbulence are a critical necessity.

Various confinement modes exist in a tokamak as the power of the heating source is increased. The most well-known one is the L-mode *(Low confinement mode)*, but it is only the H-mode *(High confinement mode)* the one that brings some hope to the idea of industrial fusion processes. Still, there are many unknowns to the dynamic processes that take part in this last regime.

In H-mode, a transport barrier created by the poloidal rotation of the plasma is known to appear at the edge of the tokamak section. The differences in radial velocities in this barrier, create zonal shear flows that shear apart turbulent eddies, reducing the transport of particles out of the tokamak. It is this mechanism that makes H-mode the most reasonable regime in which a fusion reactor would operate.

Still, the transport dynamics of H-mode are not fully understood. In order to make effective predictions on confinement control strategies as well as the cost and size of a future fusion energy plant, the ultimate concepts on the interaction of shear with turbulence have to be clarified. It is a proved fact that the dynamics of transport in fusion plasmas is not diffusive. Instead, the transport regime operating in L-mode appears to be similar to ”SOC dynamics” *(SOC = Self Organized Criticality)*, characterized by the existence of memory as well as the absence of characteristic scales or times. This absence makes the quest for an effective coefficient of diffusion a useless work.

As a first step towards the understanding on how the relations between turbulence and shear change the transport dynamics in H-mode, the present project aims to create an abstract model of radial turbulent transport inside tokamaks. This model needs to be versatile enough to introduce and detect essential changes and fundamental relations in the transport dynamics of the system. With it, fundamental questions such as the search for a proper effective description of transport beyond usual diffusion could be investigated in the future.

For this purpose, the running sandpile, a model that attempted to capture the basic dynamics of the plasma in L-mode introduced in the 1990's, is used and modified by introducing in it a new variable, shear. By doing this an "extended sandpile model" is created. In order to introduce the interactions of the shear with the other variables in the model in a way inspired by the actual physics in H-mode, new dynamic rules are implemented and included in a newly designed algorithm created with the software tool Matlab. This "Extended sandpile model" has then been tested by analyzing data retrieved from its continued operation.

The tool that has been used to examine the validity of this extended model is known as "transfer entropy", a tool capable of determining the direction and importance of causal flows between variables. Variables such as the instantaneous variance of the average shear, the instantaneous variance of the average gradient and the instantaneous number of unstable cells have been tested by this tool, revealing reverted relations in causality between the model with shear and the one without. Moreover, in the extended running sandpile the results show that shear can be made to become the most influential factor, something that was intended, since it is what actually happens in H-mode plasmas.

As a conclusion for these results follow that the procedures here conducted have been able to produce a model that is able to capture the essence of near-marginal transport in the presence of shear in a few rules and parameters. Furthermore, transfer entropy has been proved to be able to detect these changes afterwards.

As content of future research one could mention that a thorough exploration of the parameter space that defines the extended model should be carried out before selecting the operational point that would set the system closer to actual H-mode transport dynamics. Once done, this could serve as the starting point of investigations aiming at finding appropriate effective transport equations that, from previous experience with the usual running sandpile, would probably have to be based on the use of the integro-differential operators usually known as fractional derivatives.

Keywords: Plasma, Tokamak, Sandpile, SOC, model, Confinement, Transfer Entropy, Shear, Turbulence

ACKNOWLEDGEMENTS

To professor Raúl, without whom this work would have been unimaginable. Thank you for your dedication, your good will and the time you have devoted to this job. I very much hope that many other students will be as fortunate as I was to be in your lectures and learn from you. Thank you for teaching me about fascinating science fields that I did not know about and thank you for having the patience to do so. Your kindness, hard-working spirit and serenity will be an example to me. To me, this bachelor thesis has been much more a pleasure than an obligation.

This work puts an end to a phase of my life. A phase that I believe not to have completed alone. Thanks to my family for your encouragement and tranquility. I get peace of mind whenever I think about you. Thanks to Lu, who has crossed the sky on countless planes this year. Every effort that you made for this work to be better is patent in these pages. I am very fortunate to share with you whatever the future brings.

Thanks to my grandmothers, I still have a lot to learn from you. And a special thanks to my grandfather, whose presence was always a source of happiness. Your memory is a gift for us.

Lastly, thanks to all my friends, this work is now part of my life and I am very fortunate to share this life with you.

Gracias

CONTENTS

LIST OF FIGURES

LIST OF TABLES

1. INTRODUCTION

1.1. Introduction to Fusion Energy

1.1.1. Fusion Reaction

Nuclear fusion is a thermonuclear process that occurs when two or more atomic nuclei fuse into heavier nuclei [1]. The difference in mass between reactants and products determines the energy released in the reaction through $E = \Delta mc^2$.

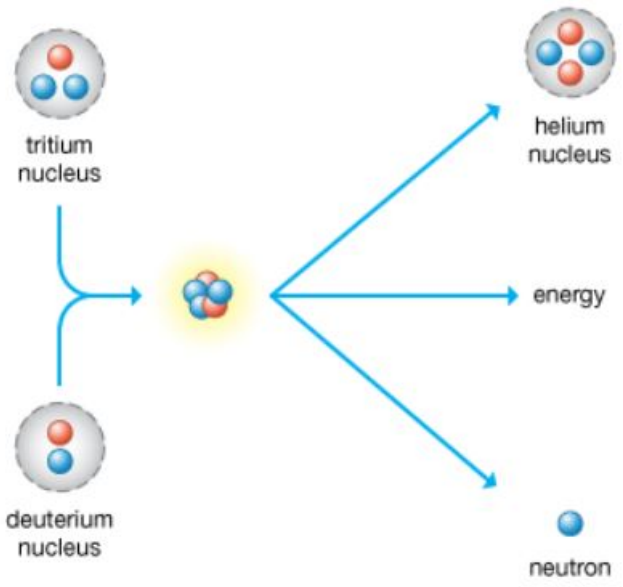

Fig. 1.1. Scheme of Deuterium - Tritium fusion reaction. Here $D_1^2 + T_1^3 \longrightarrow He_2^4 + n_0^1 + 17.6MeV$ [Encyclopaedia Britannica, Inc online site. *www.kids.britannica.com*]

For a fusion reaction to take place, nuclei have to come together. This means that atomic nuclei positively charged need to have sufficient relative kinetic energy so as to overcome the electrostatic forces pushing them apart from each other. This is, the two nuclei have to collide at sufficient speed to overcome their mutual repulsion.

The speed of the particles and the relative kinetic energy between them is strongly influenced by the temperature of the plasma. Temperature increases the probability of a successful reaction between two reactants to take place. This probability is quantified in terms of the **cross-section of the process** $\sigma(v)$ where v is the relative velocity between reactants. The **reactivity** of the reaction $\sigma \cdot v$ is therefore also dependent on the temperature of the plasma and it is directly proportional to the energy produced in the reaction.

1.1.2. Fuel for Fusion Energy production

Figure 1.2 shows that among a set of candidates for fusion reactions, the pair **D-T** Deuterium-Tritium (two isotopes of hydrogen) is the one presenting a peak for maximum reactivity (and largest energy obtention) at the lowest temperature. Therefore, for an industrial fusion reactor the D-T pair seems to be the best of choices and it is in fact the fuel planning to be used in fusion plants in the future.

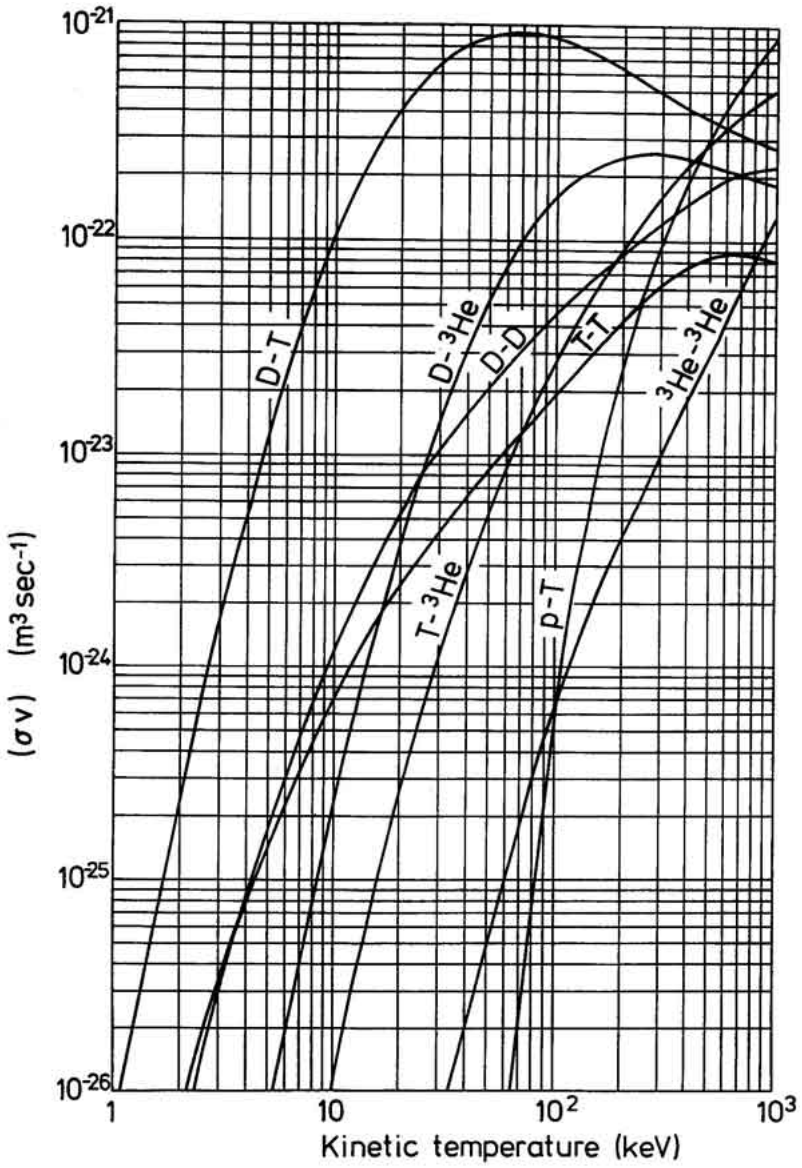

Fig. 1.2. Reactivity σv as a function of temperature for several fusion reactions. [Kaye Laby online site. National Physical Laboratory. http://www.kayelaby.npl.co.uk]

The Coulomb barrier of electrostatic forces is easier to overcome for isotopes of hydrogen as their nuclei contain only one proton. In any case, even with the lighter of elements, hydrogen, fusion is not easy. The kinetic thermal energy that the particles require can only occur at temperatures of about 150 million degrees. Considering that the

centre of the sun is at about 15 million degrees, the hottest point of the solar system would in fact be a fusion reactor on Earth and not the Sun.

At these very high temperatures, the reactant atoms separate into electrons and nuclei so that it becomes a plasma [2], an ionized gas which is sensitive to electric and magnetic fields. This sensitivity is often taken advantage of to confine the plasma into vaccuum chambers where fusion takes place.

1.1.3. The triple product

The performance of a fusion reactor candidate holding an ionized plasma is summarized in what is called "The triple product $nT\tau$" where n stands for density, T for temperature and τ for confinement time. In order to meet the Lawson criteria [3] and assure that the energy obtained from the fusion reaction overcomes the energy losses, this triple product must be greater than a specific value [1], which is

$$n \cdot T \cdot \tau \geq 3 \times 10^{21} \qquad [KeV \cdot s/m^{-3}] \tag{1.1}$$

The temperature of the plasma has been previously fixed to provide the greatest efficiency at the lowest temperature. Then, to reach first break-even and then ignition, there are two parameters left than can be adjusted: density and confinement time τ.

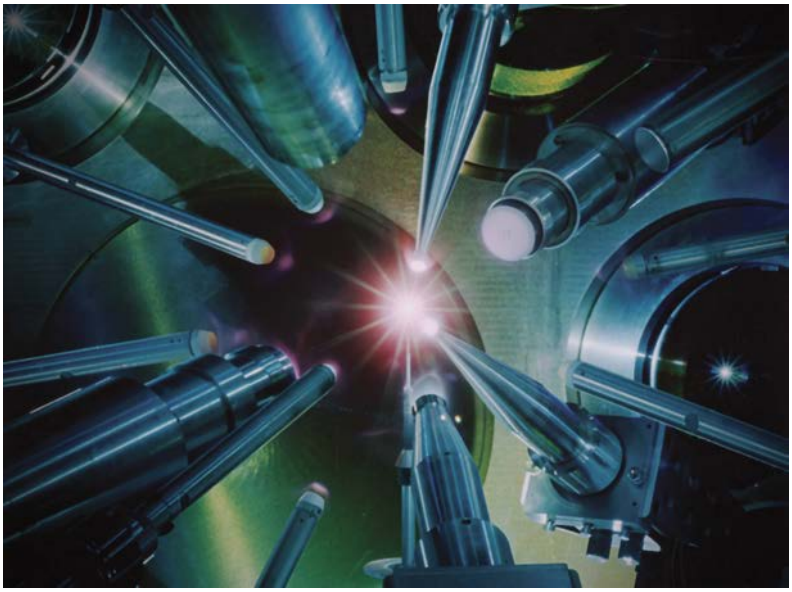

Fig. 1.3. Laser tools in ICF device. [National ignition facility. Lawrence Livermore National Laboratory]

These two parameters have led to two distinct types of fusion reactor concepts: The ones that aim to increase density at reduced confinement time (Inertial confinement Fusion **ICF** [4], see fig 1.3) and the ones that aim to increase confinement time at lower densities by taking advantage of the plasma sensitivity to magnetic fields. This is, magnetic confinement fusion **MCF** [5]. Examples of devices that exploit this last approach

are Stellarators [6] and Tokamaks [7], that compete to provide be the most reliability and stablility to the confined plasma. Figure 1.4 shows these two typologyes.

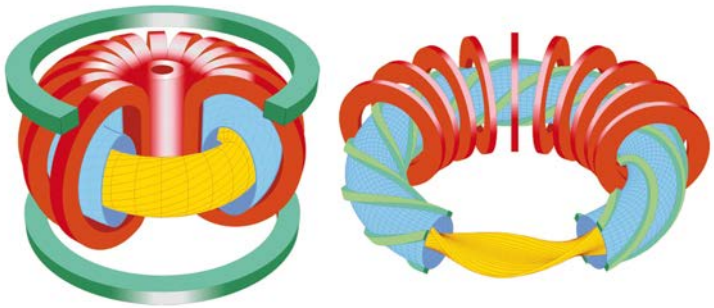

Fig. 1.4. Tokamak (left) and Stellarator (right) schemes. The plasma with its magnetic field lines is shown in yellow, magnetic coils are drawn in red and the vaccuum chamber in blue.

As it is seen in the above picture, Tokamaks present a simpler geometry and symmetric properties while the construction of Stellarators involves greater complexities. Tokamaks have been widely used for fusion research over the past years, even motivating international collaboration in one of the most ambitious programmes of the century: the construction of **ITER** (see Fig 1.5), the largest Tokamak in Earth to prove the feasibility of fusion as a reliable source of energy. This paper focuses on the investigation of transport phenomena taking place in the turbulent plasma in tokamaks. In order to examine this issue, a more detailed insight on tokamaks will be addressed in the following section. What is really a Tokamak? What happens to the plasma inside a Tokamak?

Fig. 1.5. Construction site of ITER project, late 2017 [Credits: ITER Organization online site www.iter.org]

1.2. Tokamaks

As it was mentioned before, the fuel (D-T) used in the tokamak is heated up to temperatures of 150 million degrees. In these conditions, the fuel is no longer a gas, but a "plasma" which is ionized and therefore sensitive to magnetic fields. Even if it may seem that achieving these extreme temperatures is the difficult part of the process, what is really challenging is not the heating of the plasma but confining it and keeping it stable. Tokamaks attempt to reach this goal. There is no material or physical box that could deal with plasma at such temperatures without undergoing severe damage. Also, the contact of the plasma with any "cool" walls would decrease abruptly its temperature and spoil the fusion reactions. The solution is to confine the plasma in a magnetic cage formed by superconductive magnets that are cooled with liquid helium and prevent in this way contact of plasma with the walls. This concept is called "Magnetic bottle" and it was developed in the 1950's [5].

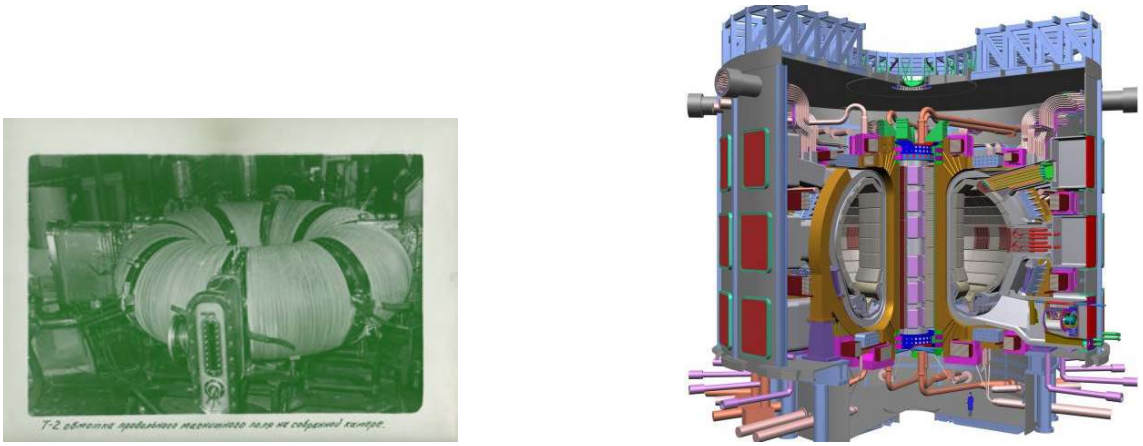

(a) Soviet Tokamak T-2

(b) Tokamak in ITER project, blue person for scale at the bottom

Fig. 1.6. Examples of evolution of Tokamak design. [Credits: *www.tokamak.info* & ITER online site *www.iter.org*]

The word Tokamak was originally an acronym for the description in russian "toroidal chamber with magnetic coils". This type of device was invented by soviet physicists Igor Tamm and Andrei Sakharov in the 1960's . From that point on, tokamaks have been widely used in nuclear fusion investigation and their design has been improved, being ITER the most ambitious project in this field, which is under construction today.

1.2.1. How does a Tokamak work?

If an electric current is passed through a wire, it generates a magnetic field which is perpendicular to the direction in which the current flows. This magnetic field will be followed by any ionized particles.

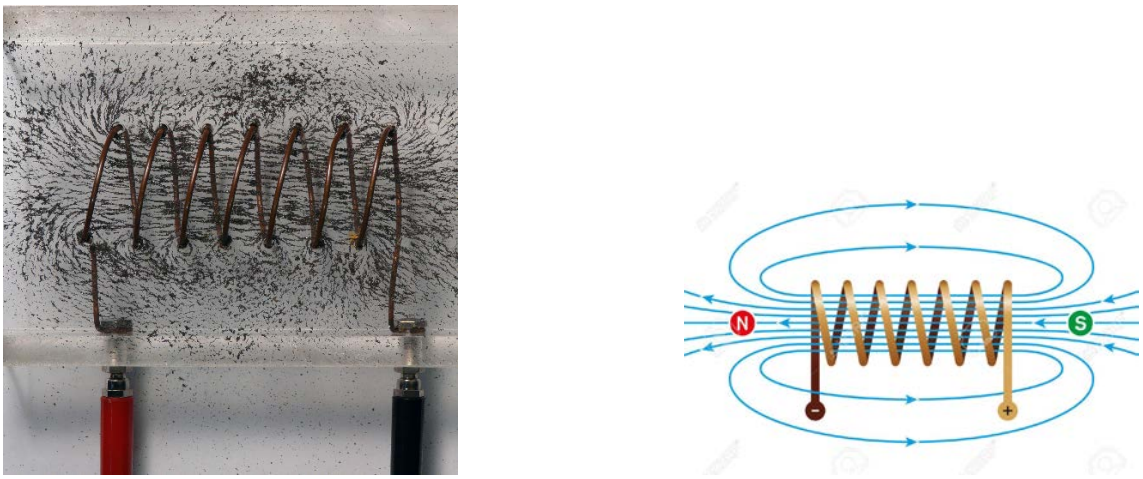

(a) Experimental Result (b) Theoretical explanation

Fig. 1.7. Magnetic fields caused by a current passing through a solenoid [Credits: TSG Physics at MIT online site *www.mit.edu*]

If the coil is closed round on itself in the shape of a donut (torus), the field lines will form a closed path in its interior. Then, the particles that form the plasma should keep rotating, they keep going around following the field lines. The bent-round-itself solenoid concept would be the equivalent to the toroidal superconductive electromagnets through which a large electric current passes, creating the toroidal magnetic field in the vaccuum chamber of the tokamak. This is the main principle of this confinement device.

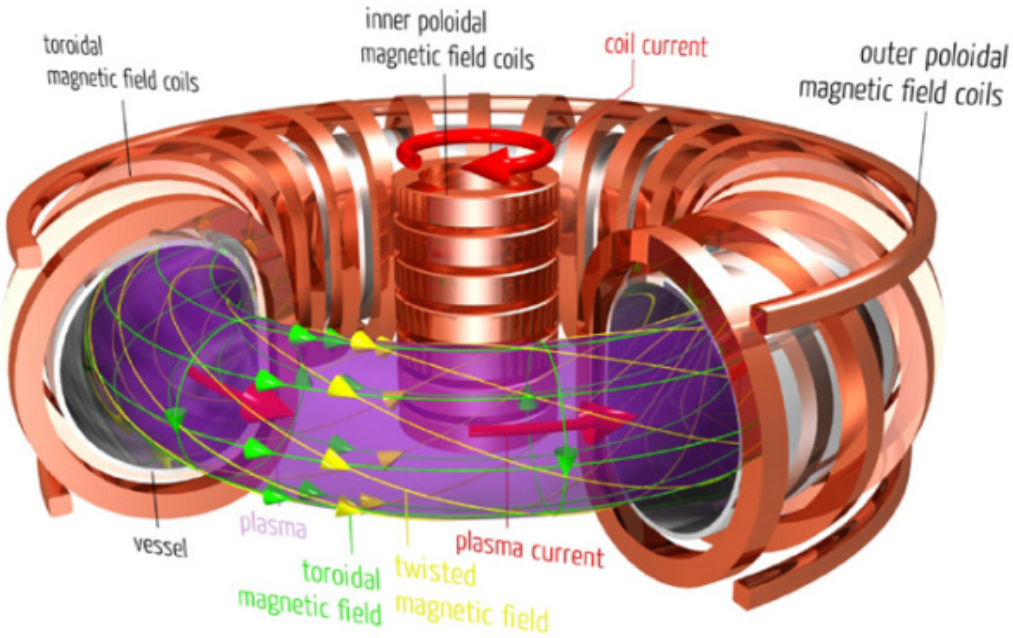

Fig. 1.8. Tokamak functioning scheme

It turns out that this magnetic field encloses complications. The plasma particles experience drift motions due to the presence of gradients and to the fact that the magnetic field is not uniform. These drifts tend to push them out of the confining device unless counteracted upon. Thus, the fuel is not well confined. To prevent this from hapenning, the magnetic field is slightly modified: Another solenoid is placed vertically in the middle of the tokamak, acting as the primary of a transformer of which the plasma itself acts as the secondary. This new element induces a current in the rotating plasma. In this way the fuel is also carrying a current in the toroidal direction that will induce a magnetic field that goes in the poloidal direction. The resulting magnetic field is composed of helicoidal field lines, which confine the plasma much better, partially cancelling out these drifts [7]. However, during the operation of these devices, it is observed that a significant amount of particles still escape out of the confinement surfaces causing a decrease in the efficiency of the device. This is due to the fact that plasma particles are subject to turbulence as a result of the large radial gradients that must be sustained in a confined plasma. Indeed, the center of the plasma is at about 150 million degrees, whilst the edge is at a few thousand. The nature of this turbulent transport of energy and particles out of the confinement surface is the basis for the motivation of this paper.

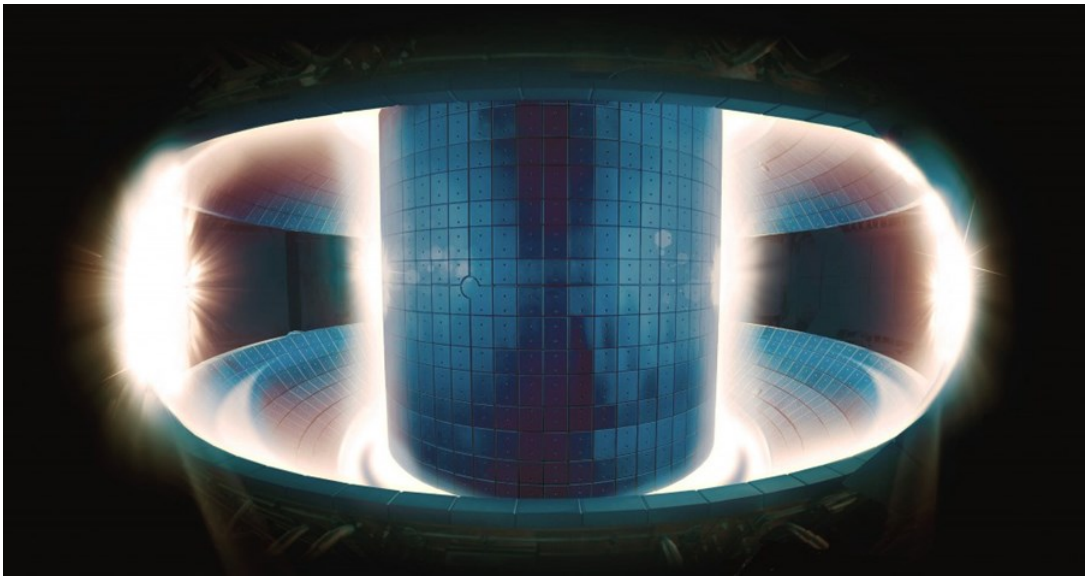

Fig. 1.9. Inside of a Tokamak vacuum chamber with plasma. The hottest points do not emit light in the visible spectrum. [Credits: National Fusion Research Institute, Korea]

2. CELLULAR AUTOMATA AND TOKAMAK TRANSPORT

2.1. Transport in Tokamaks

Let us remind that this paper bases its investigation on plasmas that are magnetically confined in order to produce fusion energy inside tokamaks. As stated before, these plasmas are subjected to strong gradients that make them highly unstable and turbulent.

Recalling the triple product $n \cdot T \cdot \tau$ that was introduced in section 1.1.3, in order for a net amount of fusion energy to be produced, the plasma has to "stay" for a certain time inside the confinement volume at a given temperature. However, the strong gradients that help to keep the turbulent rotating plasma confined drive strong electrostatic potential fluctuations. These lead to vortex structures that are aligned with the local magnetic field and drive some of the particles out of the confined volume. Thus decreasing both energy and density in the plasma and making it more difficult or even impeding fusion to take place [8].

In this regard, it is of great importance to understand the transport of particles and energy that escape the magnetic cage, since it may even make the net generation of fusion energy untenable. Yet, there are different confinement regimes in tokamaks depending on the power of the heating source. In these regimes turbulence and transport mechanisms vary. They will be presented in the following section.

2.2. Confinement Regimes in the Tokamak

In order to generate fusion energy, the plasma has to be heated up to temperatures of about 150 million degrees. As the external heating power is increased, the turbulent phenomena taking place in the plasma changes, and the radial transport of particles out of the toroidal volume changes too. This is, the plasma is known to undergo different confinement regimes [7]. The different shapes of the radial gradients of temperature and pressure that the plasma undergoes are displayed in the following figure.

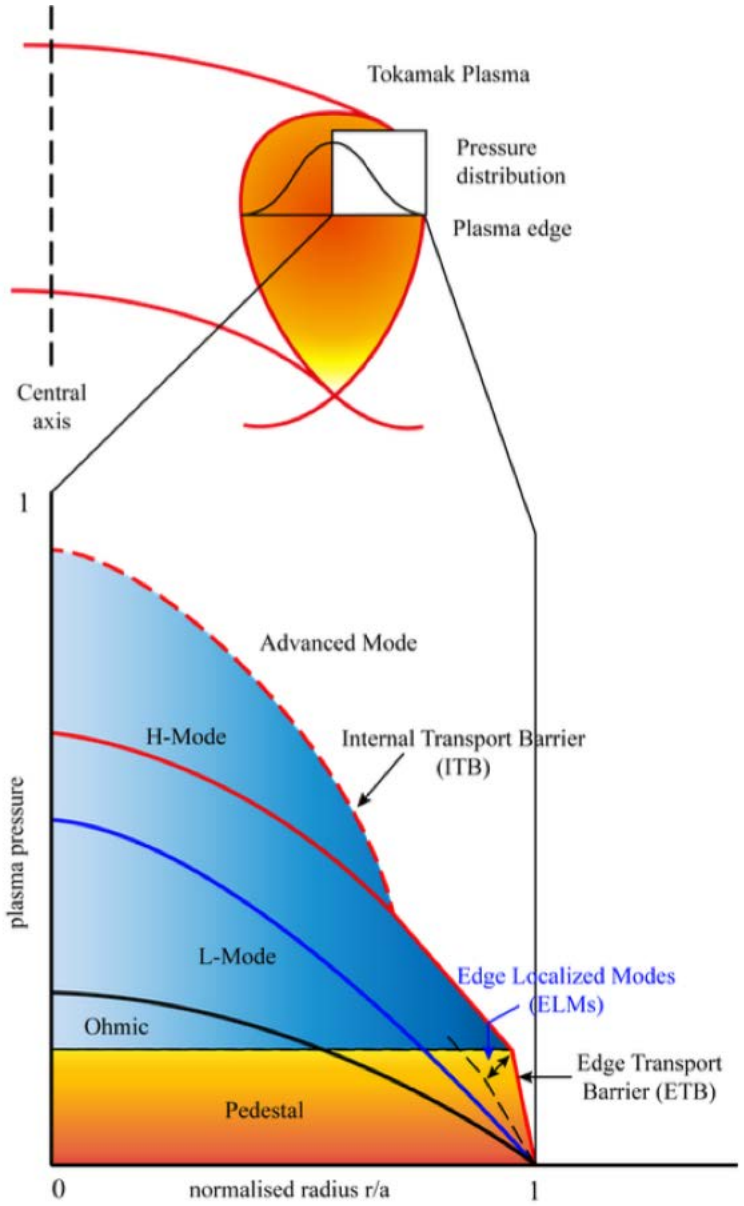

Fig. 2.1. Tokamak radial pressure profiles as the external power is increased. [Figure Reproduced from *R.Sánchez and D.E. Newman.* "Primer on Complex systems", *Springer, Heidelberg (2018)*]

In figure 2.1 three different modes are observed. As we start to heat the plasma by a procedure called *"Ohmnic heating"* [9], the pressure gradient becomes steeper and steeper up to the point in which the profile corresponding to the "L-mode" is reached. This is a very stiff profile that does not seem to respond to variations in the heating source intensity or position. However, if the plasma keeps being heated up, something suddenly happens:

A "pedestal" appears on the bottom part of the profile raising it up. This pedestal provides with some new characteristics to the profile:

1. Over the pedestal region, the profile is much steeper.

2. The gradient of the rest of the profile remains the same.

The appearance of this "pedestal" indicates that we have entered a new confinement mode, namely "H - mode" [10]. This last confinement mode entails a new hope for fusion plasma reactors. The reasons behind this statement will be explained in the following sections and the transport dynamics prevalent in these plasmas will constitute the core of the present work.

Advanced modes in which internal transport barriers are artificially created inside the tokamaks also exist, however the next-step tokamak ITER, currently under construction in France, will base its operation on the standard H-mode. For that reason, advanced modes will not be treated in the present study.

2.2.1. Cellular automata representation of the tokamak L-mode

In the L - mode, the radial gradients of temperature and pressure seem invariant to the intensity and placement of the external source. These gradients are very stiff and they do not change as the external power source is increased. This stiffness has been associated to near-marginal conditions that lead to the so-called self-organized critical (SOC) state [11], that we will discuss soon. Many studies, recently revied in reference [12], have shown that transport across the radius of the torus in near-marginal conditions obeys non-diffusive transport laws. In particular, it is believed that transport is ruled by SOC transport dynamics. In order to capture the essence of the transport phenomena and the physics of the L-mode, a successful model was introduced in 1996 based on a cellular automata called *The running sandpile*. [13]) The characteristics of this model, will be addressed below.

2.2.2. The running sandpile model

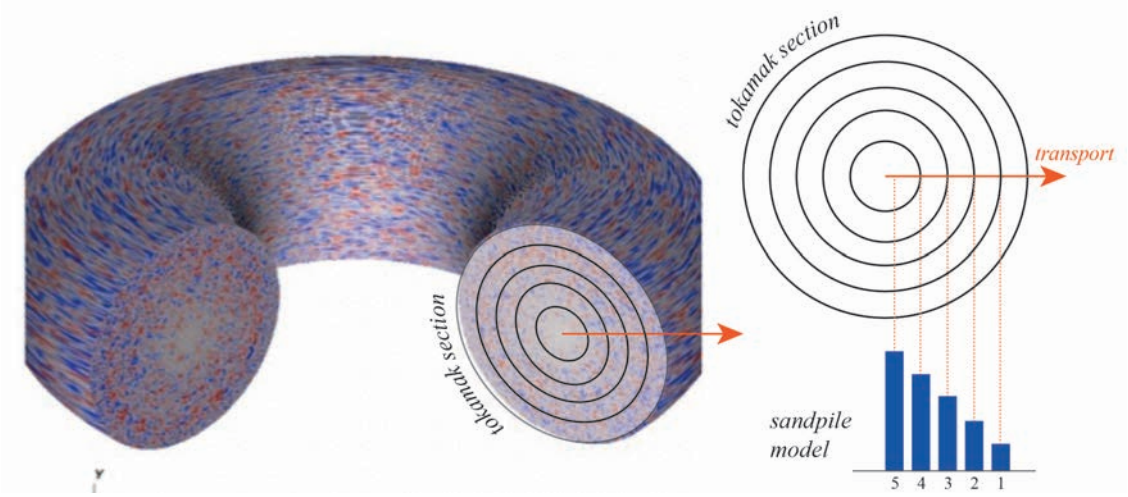

Fig. 2.2. Scheme of relation between phenomena in the tokamak and the running sandpile model

The running sandpile was proposed as a paradigm of L-mode plasmas in 1996 (Ref. [14]) as a proposal to explain the dynamics of the near-marginal transport without relying on the underlying local fluctuation mechanisms. It is a model that captures the basic principles of the system conformed by a plasma in mode-L and helps to understand the radial transport dynamics in the tokamak. An scheme of its essential functioning and what it represents is shown in figure 2.2.

2.2.3. Functioning of the model

There are N cells in which grains of sand are stored (being n = 1 the right-most cell and N the left-most cell). Keep in mind that in the analogy to fusion plasmas, these grains of sand may play the role of any physical property (for example, pressure, density or energy, among others) that can be stored in the system.

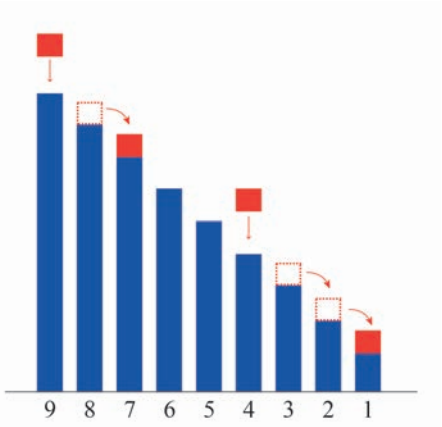

Fig. 2.3. Scheme of the functioning of a running sandpile of 9 cells

Each iteration of time starts with a rain of sand. This rain consists on a prescribed number of "N_b" grains raining on some of the cells. The number of cells that receive the "N_b" grains in each iteration is random, depending on the prescribed probability ratio "P_0" which may be, for example, 10^{-3} meaning that on average, out of a thousand iterations a cell should receive "N_b" grains once. The received grains are stored in the cells they have rained on. Each of the cells stores a number of grains until the moment in which it becomes unstable and transfers N_f grains to the cell at its right. An scheme of its functioning is displayed in figure 2.3.

The rule for a cell to become unstable is the following: If the difference in grains of the cell "n" with the cell to the right "n-1" (this is, the slope or the gradient) is greater than a prescribed threshold value Z_c, cell “n” is unstable. When this happens, N_f grains are transferred from the unstable cell to the cell that is at its right side "n-1".

After many iterations in which this process is repeated, an stationary state is reached in which the rain input balances the sand losses taking place at the bottom of the sandpile. This stationary state (the SOC state) exhibits certain ways of organization and specific events. These constitute the characteristics of the transport of grains in the sandpile, many of which can be related to the radial transport phenomena taking place in the hot turbulent plasma inside tokamaks in L-mode.

For now, let us resume the main variables and steps that model the sandpile system in the following sections.

2.2.4. Variables in the running sandpile

The main variables in the sandpile have been collected in the next table. Next to it, their counterpart in the confined plasma in L-mode are shown. The main idea here is that each cell plays the role of a magnetic surface in the tokamak, where the largest instabilities tend to appear.

The random rain corresponds to the external drive in the tokamak. The height of each cell is the value of a physical quantity say, the local pressure or density. The critical threshold in the sandpile plays the role of the critical threshold (usually, a pressure or temperature gradient) that will lead to a local instability in the plasma when over come.

As a result of this instability, plasma radial transport is induced, that will lead to a reduction of the local profile below the critical threshold. The amount of this reduction is modeled by N_f in the sandpile. This relaxations can lead to avalanches in the sandpile. Similarly, avalanches should be expected in L-mode plasmas, having been reported in some experiments [15].

TABLE 2.1. VARIABLES IN THE RUNNING SANDPILE

Name	Description	Real element in tokamak
N	Number of cells	Tokamak Radius divided by the number of rational surfaces
P_0	Probability of rain over each cell	External drive
h_n	Height of each cell n	Local pressure or energy
N_b	Grain fall on a cell	Strength of local drive
Z_c	Threshold for unstable slope	Instability local threshold
N_f	Grains transported from the unstable cell to the one at its right	Quantification of local profile flattening as a result of turbulent inertia

2.2.5. Algorithm steps in each iteration and rules of the running sandpile model

1. Rain of grains of sand

   Some of the cells will receive the N_b grains, some of them will not. This is decided according to rule 1.

   Rule 1. *There is a probability of P_0 of each cell receiving N_b grains during the rain*

   As explained before, this means that for $P_0 = 10^{-3}$, on average a cell must receive N_b grains once in every 1000 iterations.

2. Spot unstable cells

   (a) Calculate the slope or gradient Z in each location n, Z_n. This is, being h_n the height (number of grains of sand) at any location n

   $$Z_n = h_n - h_{n+1} \tag{2.1}$$

   (b) Check whether if there are local gradients Z_n exceeding the threshold. If there are, those cells are unstable. The rule for deciding this threshold is rule 2.

   Rule 2. *A cell n is unstable if $Z_n > Z_c$*

3. Relax the system

   This means, relax the unstable cells in the system according to rule 3.

   Rule 3. *The number of grains that each unstable cell n will transfer to the one to its right is N_f*

2.2.6. Example of a sandpile run

Let us use a running sandpile with the following parameter values in order to understand its dynamics and transport processes.

TABLE 2.2. VALUES USED IN THE SANDPILE RUN

Name	Value Used	Description
N	200	Number of cells
P_0	10^{-3}	Probability of rain over each cell
N_b	1	Grain fall on a cell
Z_c	200	Threshold for unstable slope
N_f	20	Grains transported from the unstable cell to the one at its right

Let us start from an empty sandpile in which all cells have no grains at iteration $t = 0$. As iterations run, grains of sand keep being stored in the system. Its mass keeps increasing as it is seen in figure 2.4. In this process, the profile of the sandpile keeps changing. This fact can be observed in figure 2.5 where two "intermediate profiles" are displayed.

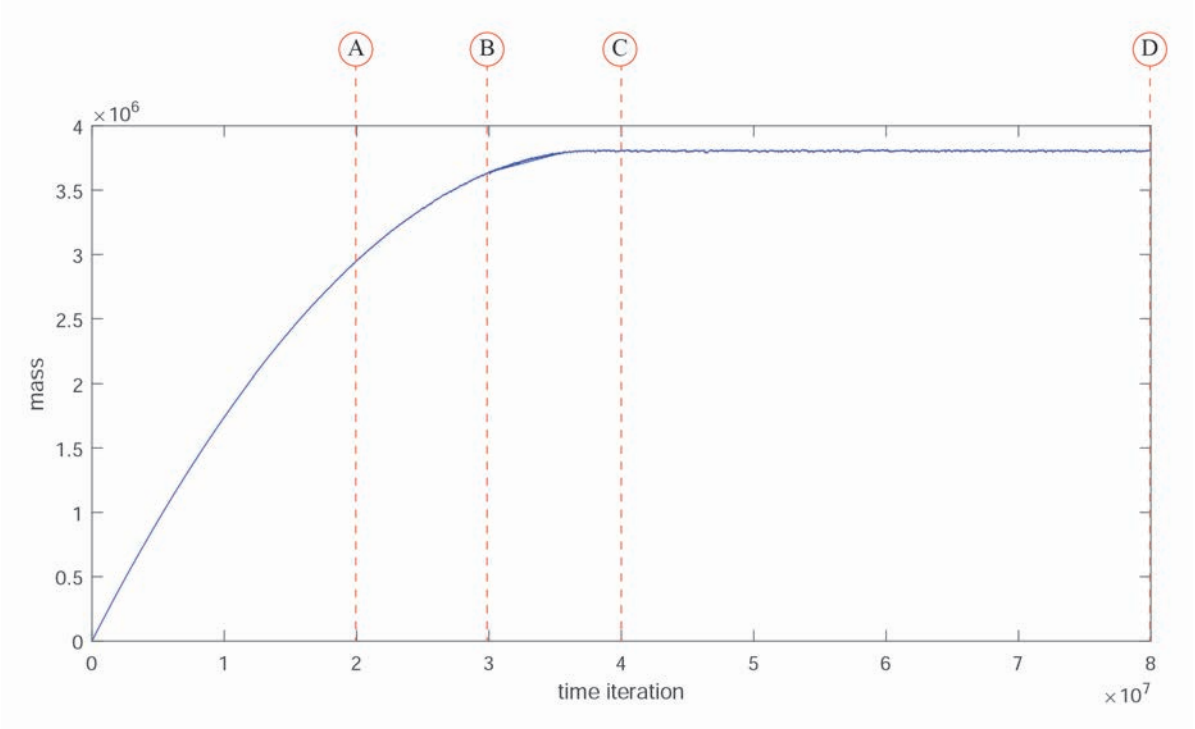

Fig. 2.4. Mass evolution in running sandpile model

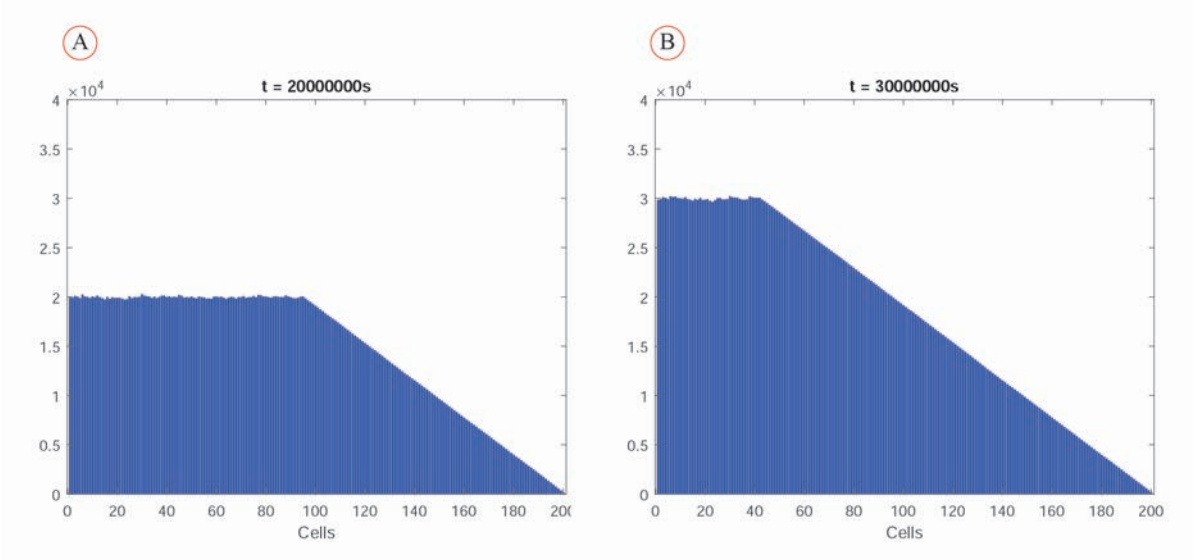

Fig. 2.5. Sandpile profiles at points A and B

It is visible in figure 2.4 that a stationary state (i.e., the SOC state), is reached in which the quantity of mass stored does not suffer great variations and maintains a rather constant value. This is reached at point ***C*** and it is visible in figure 2.6. Here, the profiles ***C*** and ***D*** are roughly equal even though they correspond to two states that are 40 million iterations away from each other.

This stationary regime is the one that exhibits the the SOC transport characteristic of the sandpile model. The behaviour of the transport of grains in this regime is analyzed in the following lines.

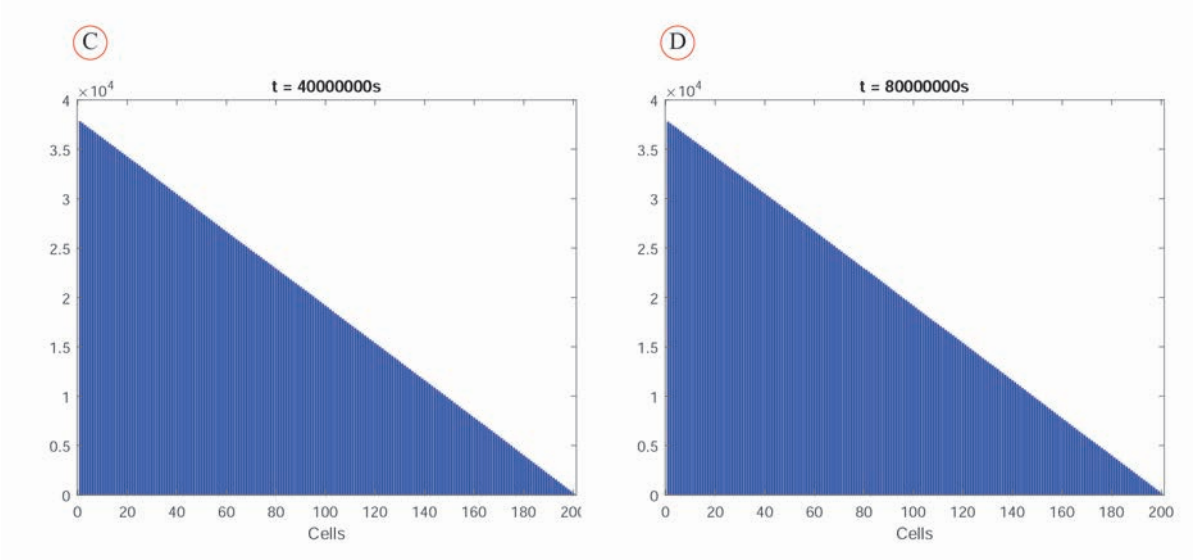

Fig. 2.6. Sandpile profiles at points C and D

Lets zoom in to a part of this sandpile and focus on a group of cells to see how they behave along the successive iterations.

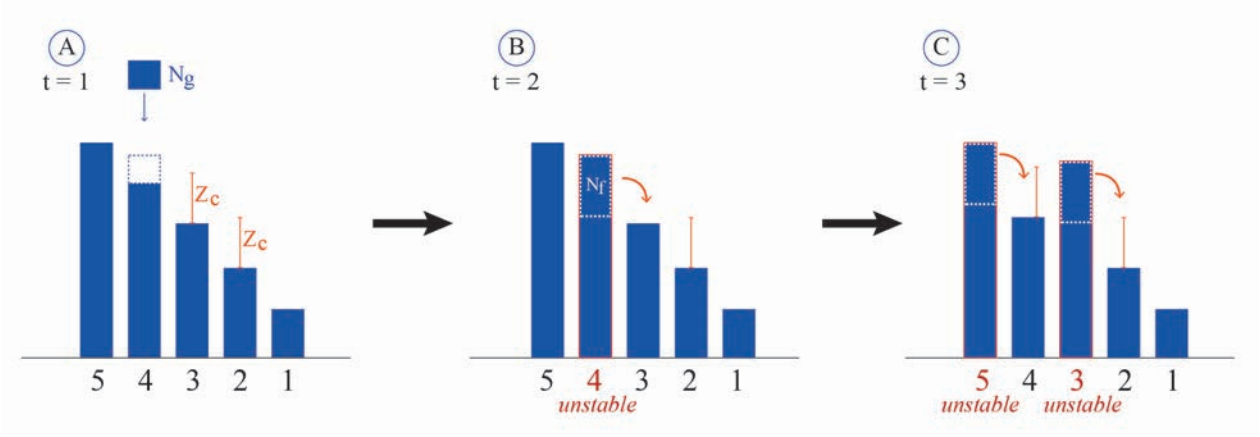

Fig. 2.7. Scheme of creation of avalanches in sandpile

A cell becomes unstable if its gradient is greater than Z_c. As shown in figure 2.7, in $t = 1$, the difference in height of cell 4 with cell 3, this is $Z_4 = h_4 - h_3$ is less than the value that would make cell 4 unstable. This means that cell 4 in $t = 1$ has still some capacity to store grains of sand before its slope surpases the critical slope and $Z_4 > Z_c$.

In this iteration, N_b grains rain on cell 4 whereas there is no rain over the rest of cells. Now, the height h_4 has increased and $Z_4 > Z_c$. According to rule 2, cell n is now an unstable cell as it is shown in part B of figure 2.7. This means that this cell will transfer to the cell to the right N_f grains of sand.

What has been described up to this point is the basic transport principle in the sandpile, which is repeatedly taking place near critical conditions (when the slope is close to be critical). However, this passing of N_f grains from an unstable cell to the one on its right is not an isolated phenomenon and has consequences on the stability of the adjacent cells in the following way.

As seen in part C of figure 2.7, since cell n passed N_f grains of sand to cell 3 in the previous iteration, this means that cell 4 has reduced its height considerably. This fact makes it now more probable for cell 5 to be unstable since the slope $Z_5 = h_5 - h_4$ is now greater than before and possibly $Z_5 > Z_c$.

At the same time, the cell to the right of cell 4, cell 3 has also been affected. It has been transferred N_f grains that have made its height higher and have also increased its slope with respect to the cell to its right. It is very possible then that cell 3 is unstable too. The procedure here described, in which an unstable cell makes the two contiguous cells to its left and right to be unstable in the next iteration, is very frequent and leads to schemes of unstable cells such as the one displayed in figure 2.8.

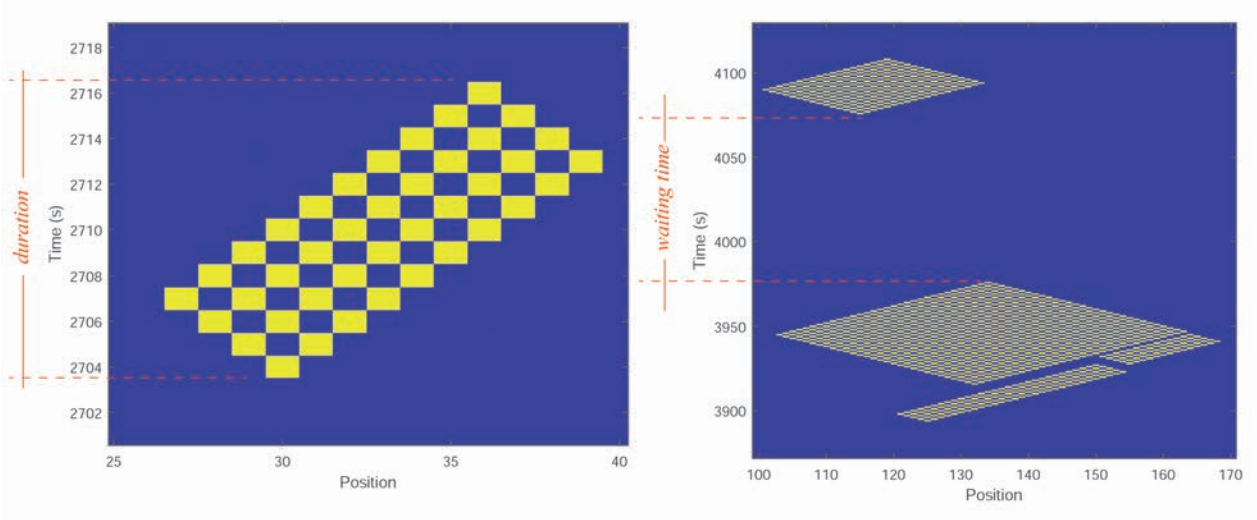

Fig. 2.8. Avalanches in sandpile

In this figure, the yellow squares represent unstable cells. It is clear that there is a group of unstable cells along some iterations that form a shape that resembles a tilted square. This is an avalanche, the characteristic transport event of this model. Many features appear in the sandpile transport due to this avalanches.These features are specific to a type of dynamics named "SOC dynamics".

2.2.7. Dynamics of transport in the SOC state

The sandpile model exhibits properties which are characteristics of SOC dynamics. These are the following [1]:

1. The system reaches a stationary state by itself. Thus, the use of the term ”self-organized”. In this stationary state the mass of the system (the number of grains of sand) remains constant on average. This means that the mass that has been introduced in the system is driven out of it. This state is reached at point ***C*** in figure 2.4. Figure 2.9 shows how the system initialized with a profile which is near the critical gradient (different to being initialized with an empty sandpile as in figure 2.4), evolves to the same SOC state on its own.

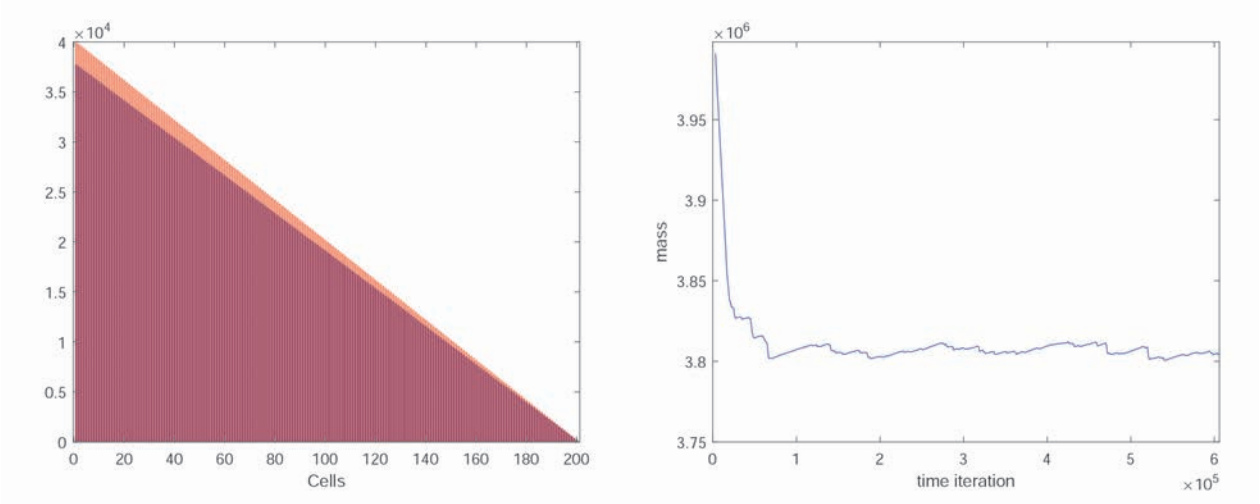

Fig. 2.9. Profile at initialization shown in orange, profile in the SOC state shown in red and evolution of the mass stored in the system shown at the right. It is visible how the system expells the excess of mass during the first iterations to reach the SOC stationary state.

2. In the SOC state, the local gradients remain close to, although on average below, the critical gradient. This can also be seen in figure 2.9, where the gradient at the initialization state (orange) was chosen to be the critical one. It is shown how after the sandpile has been run many times, the final gradient in the SOC state is very close to the critical one.

3. Transport in the SOC state is produced by avalanches. This in turn implies the following facts:

   (a) There are no characteristic scales in the system. The avalanches affect more cells if the system is larger. Their size is only limited by the sandpile size.

   (b) When transport is produced by avalanches, the scaling of confinement time with the system size is worse than than in the case of diffusive transport.

   What does this mean? In order to illustrate this statement let us introduce the following figure that represents a diffusive transport process across the radial section of a tokamak:

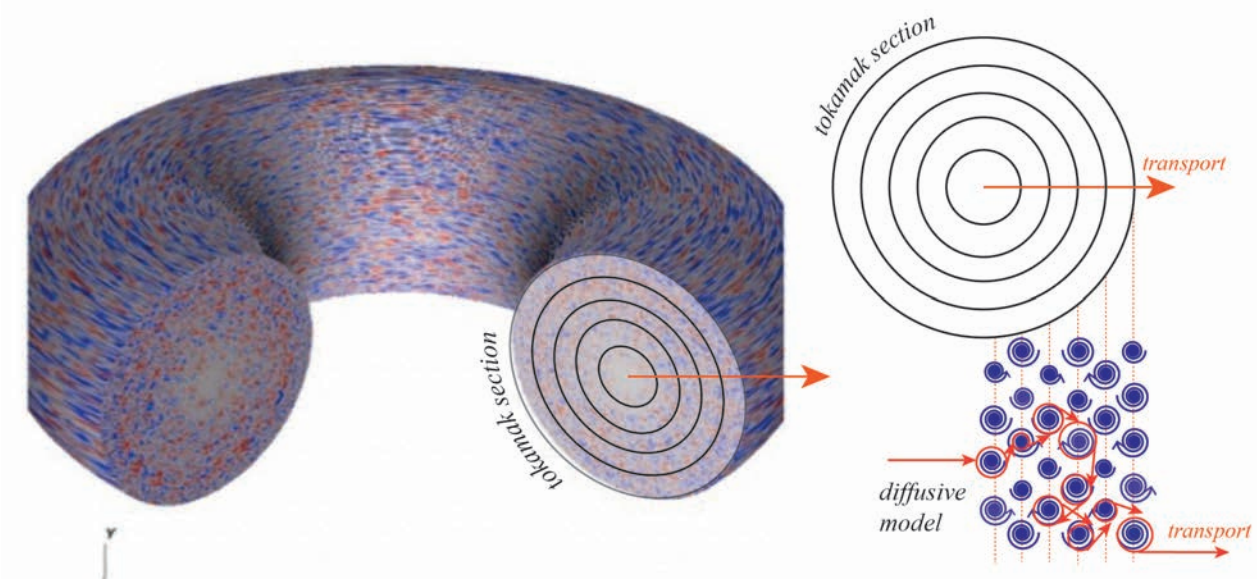

Fig. 2.10. Scheme of radial transport by diffusion

The continuous presence of turbulent eddies would make the projection on any toroidal plane of the trajectory of a particle to be erratic and go forward and backwards in radial positions before exiting the confined volume. It can be seen that this type of "diffusive transport" leads to a scaling of the confinement time $\tau \propto L^2$, being L the radius of the torus.

On the other hand, in SOC state, transport resembles Fig 2.11. It corresponds to the presence of turbulent eddies that are not ”active” at all times, but only when a cell becomes unstable. In this way, the particle does not go backwards and forward. On the contrary, it can only go forward and it can go across the section very rapidly in the case of an avalanche. This makes the confinement times shorter in the ”SOC” case than in the diffusive case.

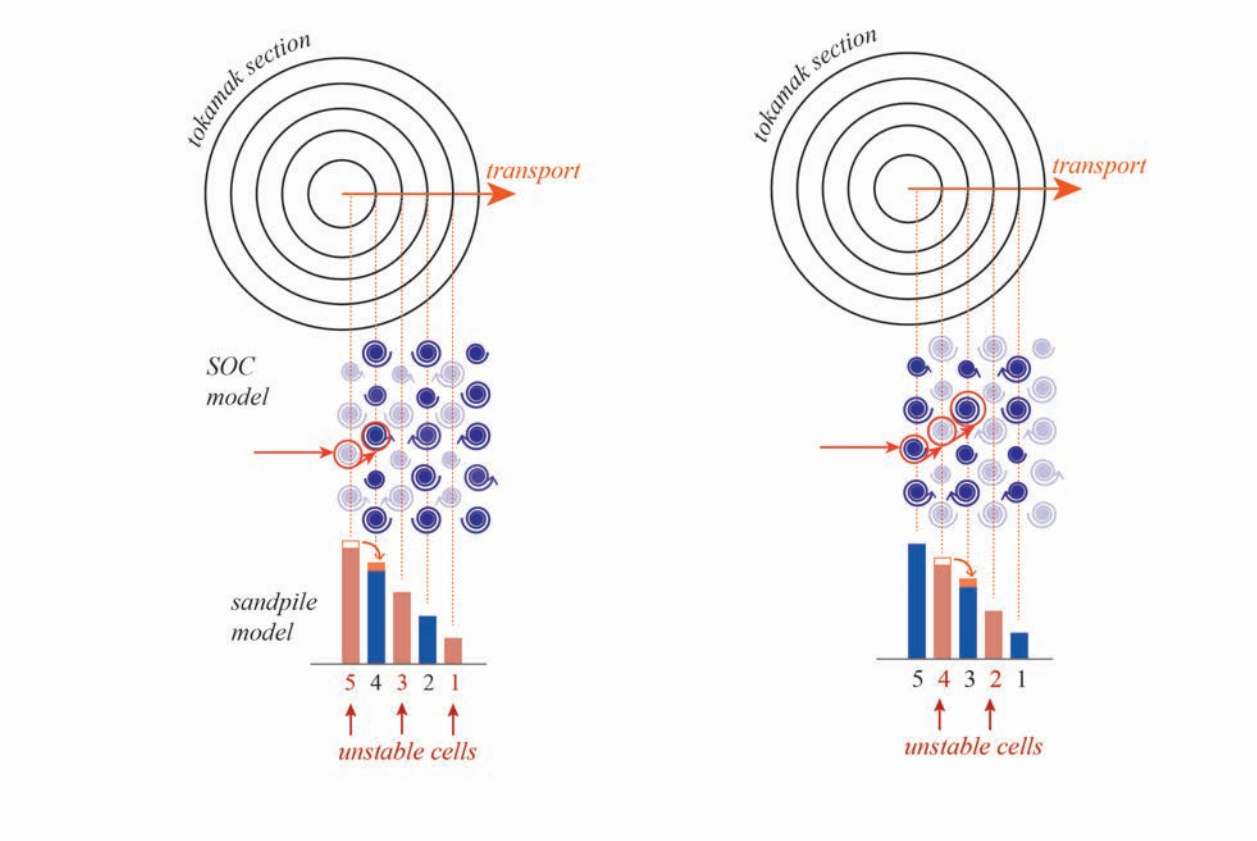

Fig. 2.11. Scheme of radial transport by avalanches

The scaling of the confinement τ obbeys the following law:

$$\tau \propto L^a \tag{2.2}$$

where L is the sandpile size. The exponent a is closer to 1 in the case of SOC dynamics.

In practice, these scaling laws are very important. For instance, in order to quadruple the confinement time, a "diffusive sandpile" would need to double its size, whilst we would need a "SOC sandpile" that is four times larger.

4. There is memory in the system. Memory is stored in the profile. The height of each cell is a direct consequence of the events that took place in the previous iteration. Be it a hole (in case the unstable cell transfered N_f grains) or a bump in case the cell received N_f grains from the contiguous one. This will directly affect when, where and how large the next avalanche will be. This memory is active for very, very long times.

The aforedescribed sandpile was introduced to try to understand the consequences of SOC-type transport dynamics in L-mode tokamaks.This is not a trivial question, since SOC-type radial transport dynamics, if present, may lead to much more expensive reactors, since the price tag scales with a power between 2 and 3 of the tokamak minor radius!

In addition, SOC-like dynamics would require the use of non-diffusive transport models to predict the performance of these devices. The usual classical diffusive equation would no longer be adequate and new mathematical tools need to be devised. Current research, based on the extensive used of sandiple models like the one just described, suggest that these models might need to be based on integro-differential operators known as fractional derivatives, that provide an interpolation between our usual (integer) derivative and integral operators [12].

2.3. H-mode transport dynamics

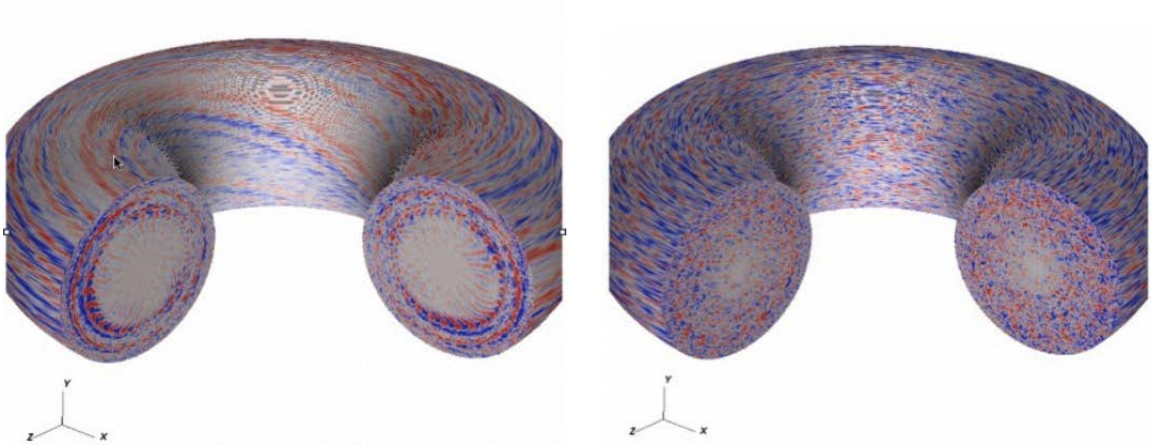

Fig. 2.12. Computer simulations of tokamak turbulent structures in H-mode

As it was introduced in section 2.2, when the plasma is heated beyond the stiff L-mode, there is a minimum power above which it suddenly rearranges itself in a new profile corresponding to the H-mode. The resulting profile rearrangement can be observed in figure 2.12.

The H in H-mode stands for "High confinement". It is a strong and sudden change in plasma characteristics that is still not fully understood [10]. Even though the inner part of the radial section behaves in the same way as in L-mode, a transport barrier is known to appear at the edge of the radial section *(ETB Edge transport barrier)* reducing the rate at which radially transported particles escape the volume.

The origin of the ETB seems to be related to the poloidal plasma rotation that is driven by the strong turbulences on the external layers of the toroid [16].

This rotation is differential, each radial position of the radial section is rotating with a different speed. The gradient of these speeds is what is called shear. The flow is then known as shear flow or zonal flow. This shear acts on turbulent eddies that are transporting particles radially out of the tokamak by stretching and shearing them apart. It is believed by many that this reduction in size, among other things, is the dominant mechanism of confinement improvement [17].

It is visible in the left part of the simulation in figure 2.12 how the plasma is rotating in the poloidal direction. In the right part of the figure the state that results as a consequence of this fact is shown. Here, the turbulent structures have been sheared apart, exhibiting much smaller radial sizes.

Figure 2.13 is an skematic representation of the implications of this in the section of the tokamak. As seen in the right part of this sketch, turbulence is sheared out by the external transport barrier. This fact entails consequences for transport dynamics in the system that are detailed in the following section:

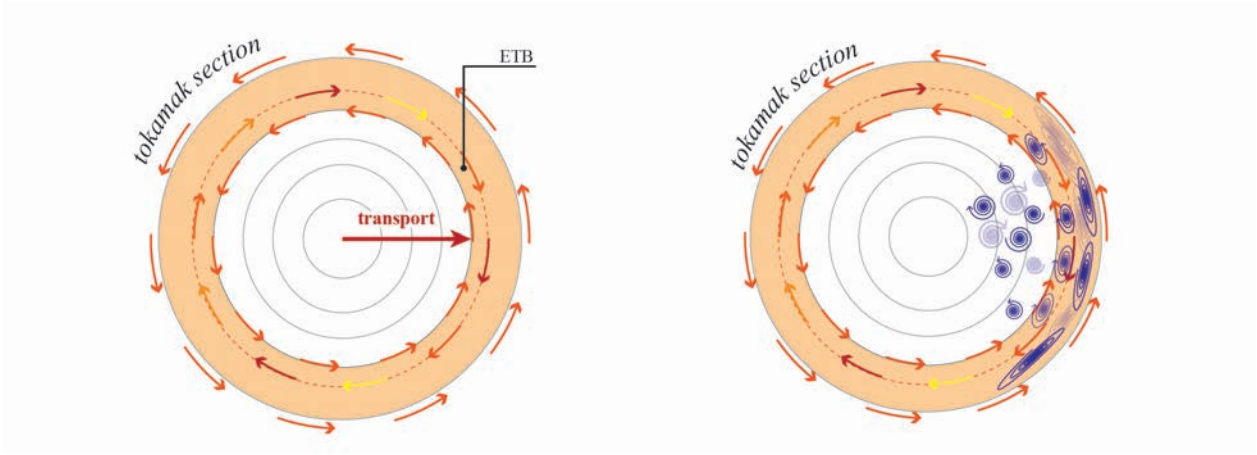

Fig. 2.13. ETB and its effect on turbulence

2.3.1. Consequences of the appearance of the ETB

The main consequences of the appearance of the ETB and zonal shear flows are the ones listed below:

1. The confinement time increases since the turbulent eddies responsible for transport are sheared apart by the shear flows as seen in the right part of figure .
2. The radial profile becomes steeper at the barrier, and raises on top of it. As a result, the system is able to store more particles due to the better confinement properties.
3. Better scaling properties than in the L-mode. As it was introduced in the previous section, in the case of SOC dynamics the the confinement time is expected to scale as dictated by the rule $\tau \propto R^a$, where in the case of SOC dynamics $\tau \propto R^1$. However, when the H-mode emerges this scaling changes to $\tau \propto R^{1.8}$ which is much closer to the diffusive case.

TABLE 2.3. SCALING OF THE LENGTH R DEPENDING ON TRANSPORT DYNAMICS

	Diffusion	**SOC in L-mode**	**H-mode + ETB**
Exponent a	2	close to 1	1.8
Scaling of L in order to quadruple confinement time	2 times larger	4 times larger	2.15 times larger

The confinement properties in this mode are known to be much better, yet the physics behind it are still not fully understood. The proper understanding of this mode constitutes a crucial factor to the future of nuclear fusion. A better confinement means that a smaller tokamak will be needed. This in turn implies a reduction in costs that could make fusion a reliable source of energy.

3. MOTIVATION OF THE PROJECT

3.1. Main objectives

The better confining characteristics in H-mode have made it the regime in which tokamaks will probably operate in the future. Or at least, that is the regime in which the next-step tokamak, ITER, currently under construction in Southern France will operate.

For that reason, and following the work done for the L-mode using the running sandpile, the objective of the project is to design a cellular automata that captures the basic dynamics of the H-mode in fusion plasmas inside tokamaks

If successful, this extended sandpile could be used in the future to carry out similar scaling studies and to look for adequate mathematical formalisms to describe transport that will help to predict the confinement properties of tokamaks.

For this purpose, it is essential to capture the way in which turbulence interacts with shear to change the transport dynamics. The starting point will be "the running sandpile" already introduced in the previous section which has been proved to reproduce the essential physical principles of the L-mode.

Therefore, this project will pursue three main objectives:

1. Design an extended sandpile model that incorporates the essentials of how shear flows in H-mode change the characteristics of transport with respect to L-mode. This new model should give an insight on the ways in which turbulence is affected by the emerging shear flows and also on how shear flows are driven by turbulence and slowed-down by friction. For this purpose, new variables and rules have to be incorporated to the existing running sandpile model.

2. Write a code that implements the new sandpile model. This code will be created in the computer software environment Matlab ®.

3. Characterize the results obtained from this new model and compare them to the ones obtained from the running sandpile without shear. In particular, we need to be sure that the dynamical relationships between flows, turbulence and profiles are properly captured by the rules chosen. To this effect, an statistical tool known as transfer entropy [18] will be later presented and used.

3.2. Definition and aim of a model

In order to understand the physical interactions between turbulence and shear, complex quantitative simulations of a tokamak could be made. These would consist on replicating

each component of the tokamak, simulating individual local fluctuations and making a literal simulation that retrieved the data to analyze.

This is not the objective of our model. What we are looking for is an alternative and simplified representation of the system under study whose aim is to capture the underlying mechanisms and the basic logic of the phenomena to study their role in setting the final transport dynamics and providing a simplified testbed. Once this is achieved, it will open up the possibility of carrying out scaling studies, understanding qualitatively the role played by the different dynamical elements, and assess the adequateness of effective transport models for the H-mode.

4. THE EXTENDED SANDPILE MODEL

4.1. New variables

A shear poloidal flow driven by turbulence is responsible for the emergence of the H-mode [17]. Thus, it is this shears that matters and not so much the rotation itself. That is why in the new sandpile model it is vital to incorporate a new variable to model this parameter.

This field is represented by the variable "S_n". Then, in the new sandpile model each cell will contain information of two variables:

1. Z_n - The gradient of each cell, which is related to the height difference between cells $Z_n = h_n - h_{n-1}$. The gradient tells us information about the cell being or not unstable.

2. S_n - The shear in each cell, which is related to the difference in rotation speed between two contiguous radial positions in the tokamak section.

4.1.1. Functioning of shear variable

The shear flows in the edge barrier cause the turbulent eddies near the edge of the tokamak to be sheared apart and disfigured. As a consequence, radial transport is reduced. In order to model this behaviour, the new variable S_n should operate in the following way:

TABLE 4.1. VARIABLES IN THE EXTENDED SANDPILE MODEL

Implication	**What happens in the confined plasma**	**Implementation in the model**
1	Shear is caused by turbulence	The value for shear in each cell increases when the cell becomes unstable
2	If there is no turbulence, the flow and its related shear are both reduced by friction forces.	If the cell is not unstable, the value for S_n decreases
3	Shear acts on turbulence by reducing it	The value for Z_c (critical gradient) is increased in each cell when S_n increases.
4	Shear reduces turbulence-induced transport	The value for N_f, is reduced in each cell when S_n increases

4.1.2. New rules for the shear variable

The previous section presented the operational principles of the new variable, shear, and how it affects qualitatively other variables in the sandpile. Let us now, make these relations more precise by stating the concrete rules. Remember that rules 1, 2 and 3 where presented in section 2.2.5.

- **Rule 4.** Each time that a cell is unstable, the value for its shear increases in a fixed quantity ΔS.

  This rule deals with implication 1 of the previous section.

- **Rule 5.** In every iteration in which the cell does not become unstable, the value for its shear decreases a fixed quantity dS.

  This rule is related to implication 2 of the previous section. It is important to note that $dS << \Delta S$, since turbulence can drive shear much faster than friction can remove it.

- **Rule 6.** Whenever a cell becomes unstable, its critical gradient changes in the following way

$$Z_{c_{new}} = Z_c \left(1 + f \frac{S_n}{S_{max}}\right) \tag{4.1}$$

  This rule is related to implication 3. Here, the new quantities f and S_{max} are introduced. $Smax$ represents the maximum shear that the plasma is able to withstand before becoming itself unstable. In a real tokamak, this instability would be related to a Kelvin-Helmholtz mode, that appears in fluids and plasmas above a certain amount of shear. On the other hand, f is a number in the interval [0,1] that used to adjust the range of variation of $Z_{c_{new}}$.

  By increasing Z_c it is more difficult that a cell becomes unstable.

- **Rule 7.** Whenever a cell becomes unstable, the number of grains that it transports to the contiguous cell changes in the following way:

$$N_{f_{new}} = \frac{N_f}{1 + f \frac{S_n}{S_{max}}} \tag{4.2}$$

  By reducing N_f we assure that transport is less efficient. We also reduce the effectiveness of long-term memory, since holes and bumps caused in the profile by avalanches will be smaller.

4.2. The new algorithm

The rules described in the previous section, together with those of the original sandpile, have been implemented in a new Matlab code completely from scratch. The sandpile state is defined in this new code in terms of two vectors, one that contains the height of each cell, the second containing the shear of each cell. These two vectors are updated at each iteration by applying the rules according to the flowchart shown in Fig. 4.1.

TABLE 4.2. VARIABLES STORED IN EACH ITERATION

For Each cell	Height Shear
For the whole sandpile	Total Mass Mass outflux at edge Number of unstable cells Mass input
For Transfer Entropy calculations	Local variance of the sand gradient Local variance of the shear
To start next iteration	Iteration number Profile Shear state

In order to monitor progress, the extensive graphic library that Matlab provides has been used. Output of the code is also dumped on several files in standard text format (.txt) after a large number of iterations have run. In particular, the temporal evolution of the quantities shown in table 4.2 are written on files for later analysis.

Output to file is also produced to allow the restart of the simulation, situation that is often needed in order to reach the final SOC state, or to produce data for the latter analysis.

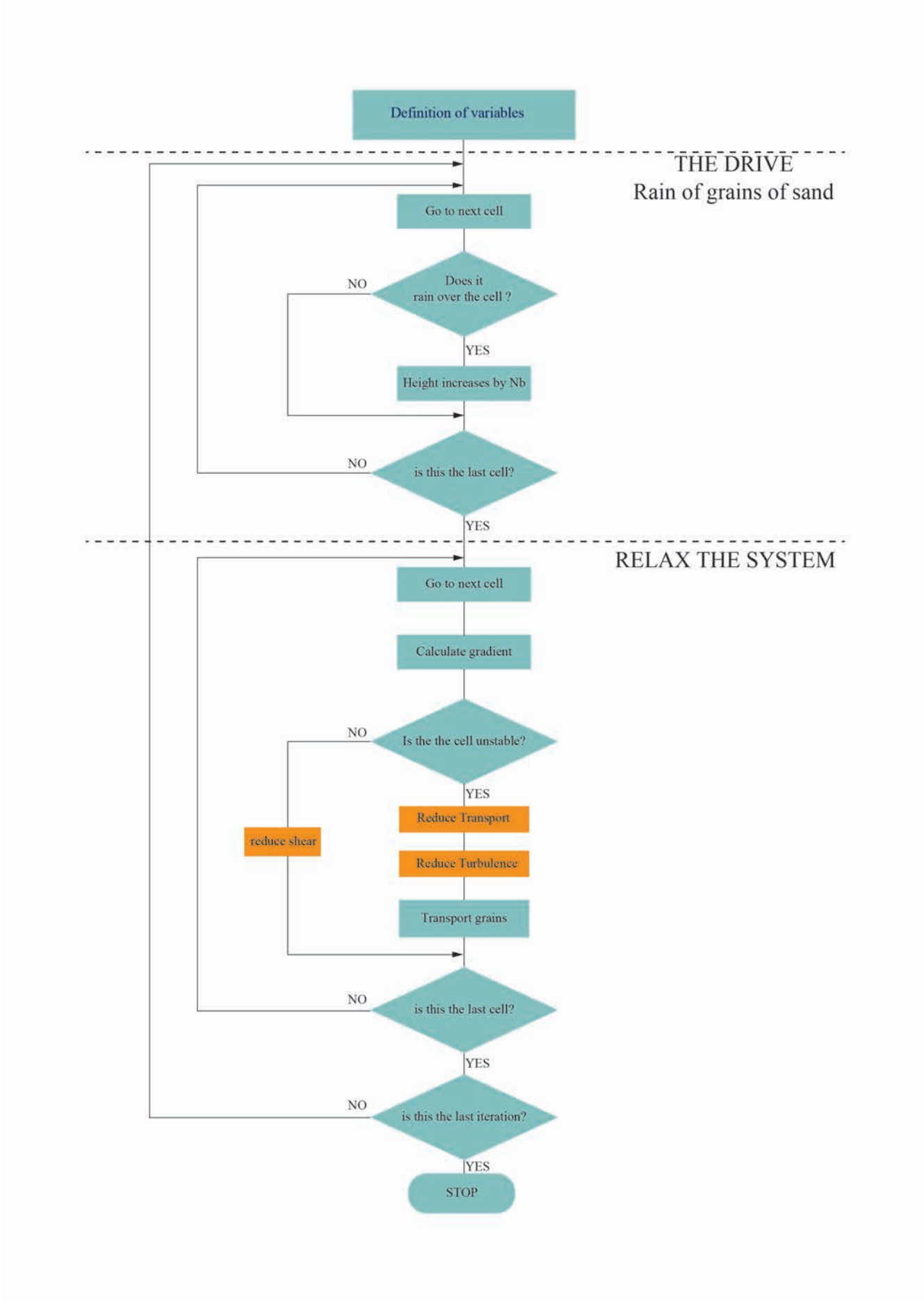

Fig. 4.1. Flowchart of the extended sandpile model algorithm, with changes related to shear shown in orange. These changes are related to rules 4, 5, 6 and 7 of the previous section

4.3. Example of an extended sandpile model run

TABLE 4.3. VARIABLES IN THE EXTENDED SANDPILE MODEL

Name	Value used	Description
N	200	Number of cells
P_0	10^{-3}	Probability of rain over each cell
N_b	1	Grain fall on a cell
Z_c	200	Threshold for unstable slope in no-shear case
N_f	20	Grains transported from unstable cell in case of no-shear.
f	0.2	Regulator for instability effect in $N_{f_{cell}}$ and $Z_{c_{cell}}$ of each cell
S_{max}	20	Maximum value of shear the system is able to withstand
dS	10^{-3}	Damping of shear in case of no instability
ΔS	0.1	Increase in shear in case of instability

A sandpile with the characteristics shown in table 4.3 was started with a gradient equal to the maximum gradient possible. This is, the case in which $S_n = S_{max}$ in equation 4.1.

$$Z_{C_{cell}} = Z_C \left(1 + f\frac{S_n}{S_{max}}\right) = Z_C\,(1 + f) \tag{4.3}$$

Since $f = 0.2$ and $Z_C = 200$, in this case the gradient of each cell will be in the interval $Z_C = [200, 240]$. To initialize this example, a gradient equal to $Z_{C_{cell}} = 240$ in every cell was chosen.

In this way, it is assured that a group of grains raining over any cell will make it go unstable. This is why in figure 4.2 it is seen that the starting tendency of the sandpile is to loose a great amount of mass.

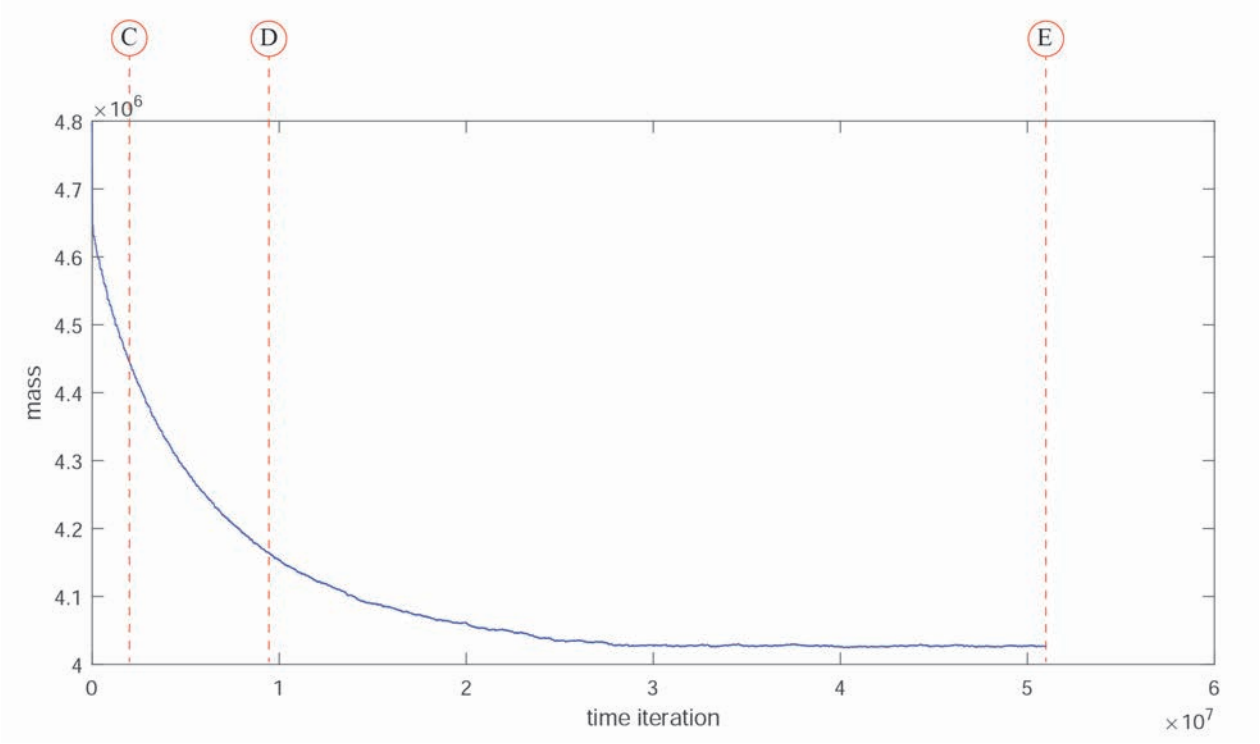

Fig. 4.2. Evolution of mass of extended sandpile model starting from a profile similiar to the critical one

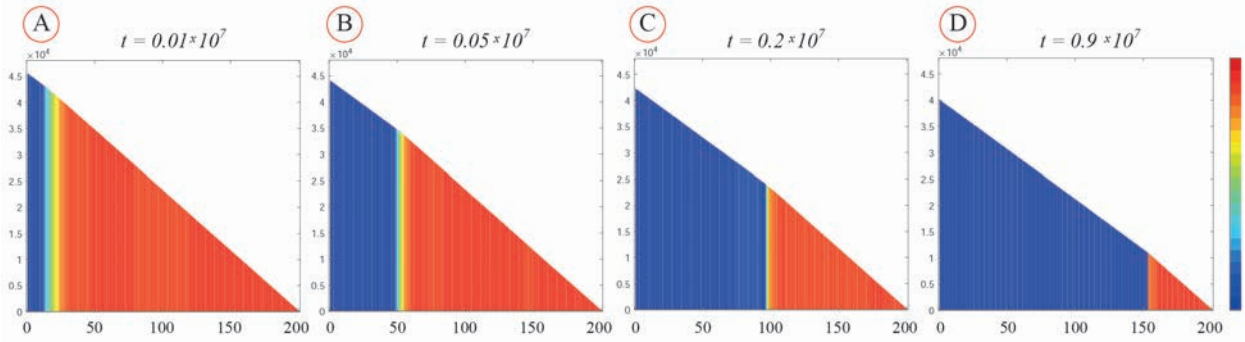

Fig. 4.3. Series evolution of shear and profile in the extended sandpile model starting from a profile similiar to the critical one. The colour bar corresponds to shear values being red the maximum shear and blue shear = 0

As the iterations keep running, the sandpile profile evolves through states **A,B,C** and **D** before reaching the stationary state **E** displayed in figure 4.5. Throughout all states in figure 4.3, it is seen that two well differentiated regions exist in the sandpile. The red region corresponds to a region with high values of shear. This is so because avalanches have been frequent in this part so that the cells here have become unstable many times. Remember that the value for shear grows each time the cell becomes unstable.

Another interesting feature of the evolution of the profile up to the SOC state is the evolution of the region that has been ”relaxed", the blue region. This region keeps expanding through the sandpile towards its end as iterations keep running. Once a cell in

this part of the sandpile has been relaxed, the time that goes by until it becomes unstable again is large enough so as to reduce its shear again to very low values. (Shear is reduced in dS in every iteration in which a cell is not unstable).

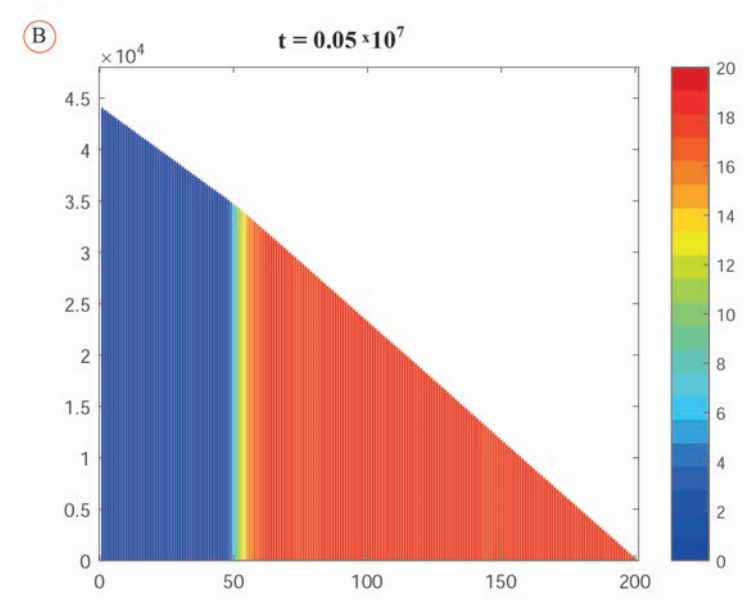

Fig. 4.4. Profile before reaching SOC state of extended running sandpile model. The colourbar represents shear values

It is visible in figure 4.4, that represents an intermediate state of the sandpile before reaching the SOC state, that the gradient is steeper in the red area. The area in this region is close to the maximun gradient possible $Z_{c_{max}}$. Both regions are separated by a thin barrier in which the values for shear change abruptly along a very small number of cells.

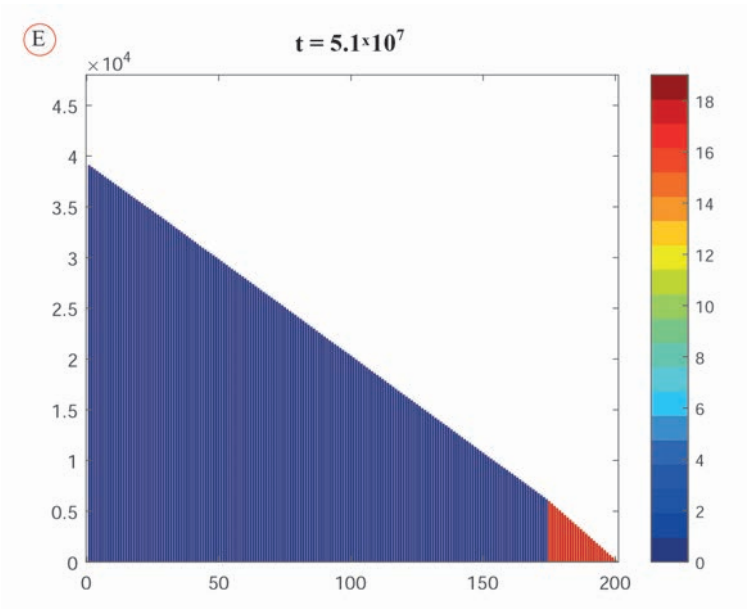

Fig. 4.5. Profile in SOC state of extended running sandpile model. The colourbar represents shear values

Figure 4.5 represents the state of the sandpile once the stationary state has been reached. The area with high shear values (red) maintains both its position and size along the following iterations. The change in gradient could resemble the change in gradient that takes place in pressure (energy) profiles at the edge pedestal that appears in tokamaks operating in H-mode.

Figure 4.6 displays the evolution of shear as iterations run when the sandpile has already reached the stationary state. It is clear the way in which shear grows when avalanches take place, reaching its highest values for the largest avalanches (the ones in which a cell becomes unstable many times). It can also be seen how in the absence of unstabilities, shear slowly decays. The same mechanisms take part in the right edge of the sandpile, however this area is subjected to more activity and so the values for shear are much greater.

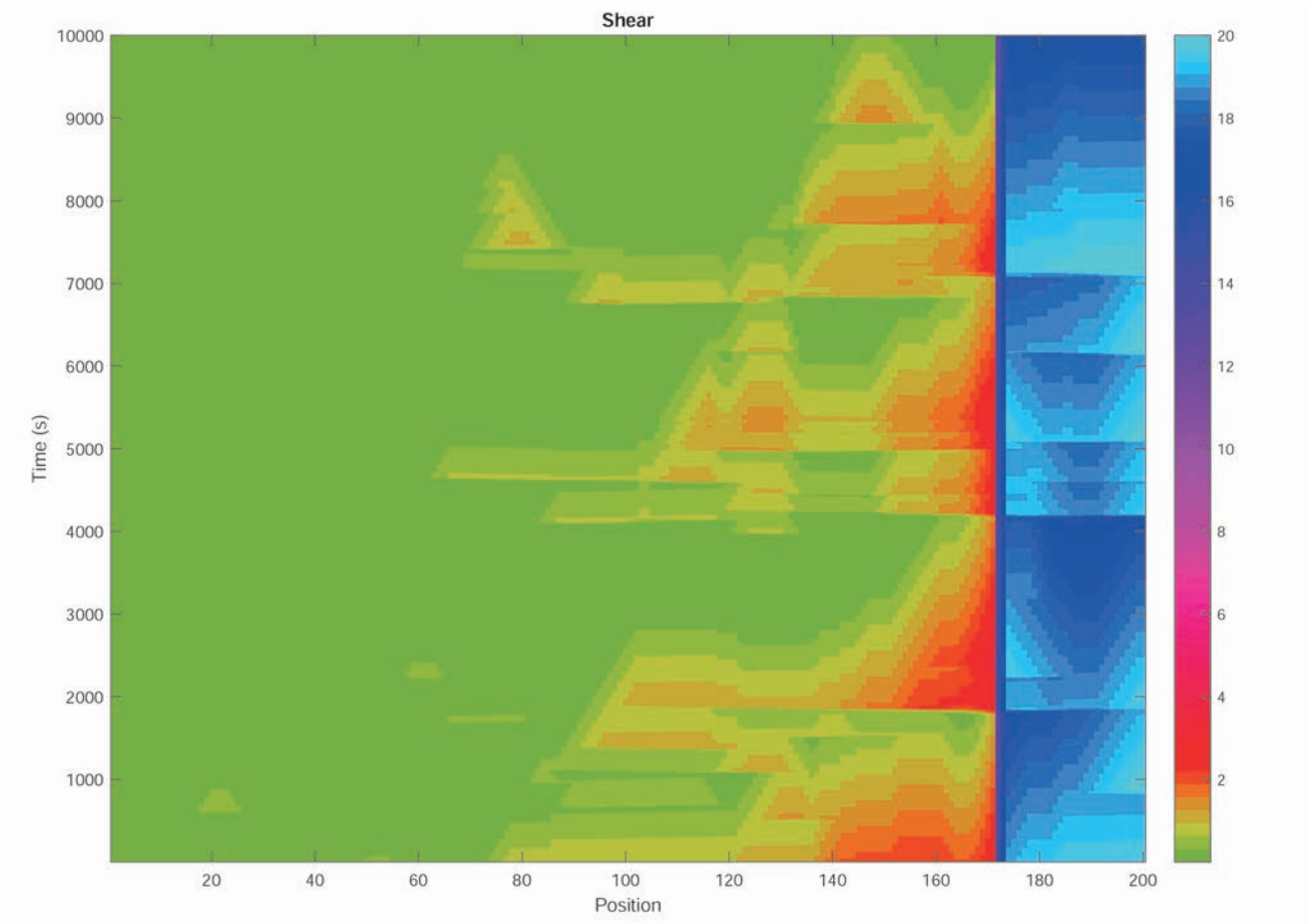

Fig. 4.6. Shear history in the stationary state of the extended sandpile model. Colour bar representing values for shear.

5. ANALYSIS OF RESULTS

The time has come to test if the new extended sandpile model is a valid tool to comprehend the basic interactions of the physical mechanisms that are thought to be important in H-mode. For this matter, data from the extended sandpile operating in its stationary state has been generated by the numerical code presented in the previous chapter and analyzed with a numerical tool aimed at providing information about the behaviour of the sandpile.

The tool that will be used is known in the physics literature as ***transfer entropy***. It quantifies the direction of transfer of information between two temporal series, which may be interpreted in many cases as a causal relationship between the physical elements that these series represent.

The information retrieved from these analysis will be compared to the suspected dynamics of the H-mode plasma inside a tokamak to test the validity of the model. In particular, we will be looking for a transfer of the dominant dynamics from the avalanche activity to the shear flow, as it is thought to happen in the transition from L to H mode in tokamaks [17].

5.1. Transfer entropy

5.1.1. Definition of Transfer entropy

Transfer entropy is a tool recently introduced in the field of Information Theory by Thomas Schreiber [18] in the following way: *For two simultaneously measured signals X and Y, if we can predict X better by using the past information from Y than without it, then we call Y causal to X.* The estimation of this transfer is done via the so-called transfer entropy, that we will introduce in the next few paragraphs.

As it is explained in Ref. [19], transfer entropy is summarized in the following mathematical expression where Y and X are two different variables whose time series consisting on x_i and y_j are to be analyzed. To evaluate to which extent Y is causal to X (To which extent changes in Y produce changes in X):

$$T_{Y\longrightarrow X} = \sum p\left(x_{n+1}, x_{n-k}, y_{n-k}\right) log_2 \frac{p\left(x_{n+1}|x_{n-k}, y_{n-k}\right)}{p\left(x_{n+1}|x_{n-k}\right)} \tag{5.1}$$

In this formula, k is the time lag index between the two time series signals being compared. By introducing this lag, one can detect the influence of one variable on the other at different time delays. That is, the effect that variable X may have an instantaneous effect on Y (k = 0), or at a much later time. The structures $p\left(A|B\right)$ express a conditional probability *"probability of A if B"*.

It is clear in the fraction of formula 5.1 that if the numerator equals the denominator (in the case that the probability of x_{n+1} is not affected by y_{n-k} so that $p(x_{n+1}|x_{n-k}) = p(x_{n+1}|x_{n-k}, y_{n-k})$) then the fraction inside the logarithmic element equals one and thus $T_{Y\longrightarrow X} = 0$. Then Y would not be affecting X.

The *"Net transfer entropy"*, which is the quantity that has been analyzed in this study is defined as

$$T^{net}_{Y\longrightarrow X} = T_{Y\longrightarrow X} - T_{X\longrightarrow Y} \tag{5.2}$$

Which means that if $T^{net}_{Y\longrightarrow X}$ is positive, $T_{Y\longrightarrow X} > T_{X\longrightarrow Y}$ and thus Y is more causal to X than X is to Y. Whereas if $T^{net}_{Y\longrightarrow X}$ is negative, the opposite happens. Also, if $T^{net}_{Y\longrightarrow X} = 0$ there is not a strong causal relation from one to the other, instead they rather affect each other in the same way. The fact of this tool providing negative or positive results reveals its directional purpose.

Transfer entropy is a rather unique tool, as it permits the analysis of variables which are extremely different from each other. This feature is quite different from other analytical tools such as cross-correlation since the latter will only yield finite values if the two time series are significantly similar for some lag value. As stated in reference 5.1, cross-correlation is maximum for two time-series signals that are identical, whereas transfer entropy between these two signals would be zero as the knowledge on one does not permit any information on the other.

5.1.2. Transfer entropy analysis of the extended sandpile model

TABLE 5.1. VARIABLES USED IN THE EXTENDED SANDPILE MODEL FOR THE TRANSFER ENTROPY ANALYSIS

Name	**Value used**
N	200
P_0	10^{-2}
N_b	1
Z_c	200
N_f	20
f	0.2
S_{max}	20
dS	10^{-3}
ΔS	0.1

In order to perform this analysis, a extended sandpile in the stationary state was tested. Data on representative variables of the sandpile model was collected and then a transfer entropy study was performed for every possible pair of the available variables time series.

The three dynamical elements that play a role in the extended sandpile are the shear, the local gradient and the local transport. The first one quantifies the role of the flow, the second one controls the excitation of instabilities when the threshold is overcome and the last one, is mediated via avalanches. The variables selected were the following:

A time series of these variables along a very extended number of iterations was collected for the analysis.

- The **Activity**, which is the total number of unstable cells present in the sandpile at each iteration. This time series produces a signal like the one shown below. It is observable here that the peaks in the signal correspond to moments of great activity, due to the presence of large avalanches. The span of time iterations without activity, are the waiting times between avalanches.

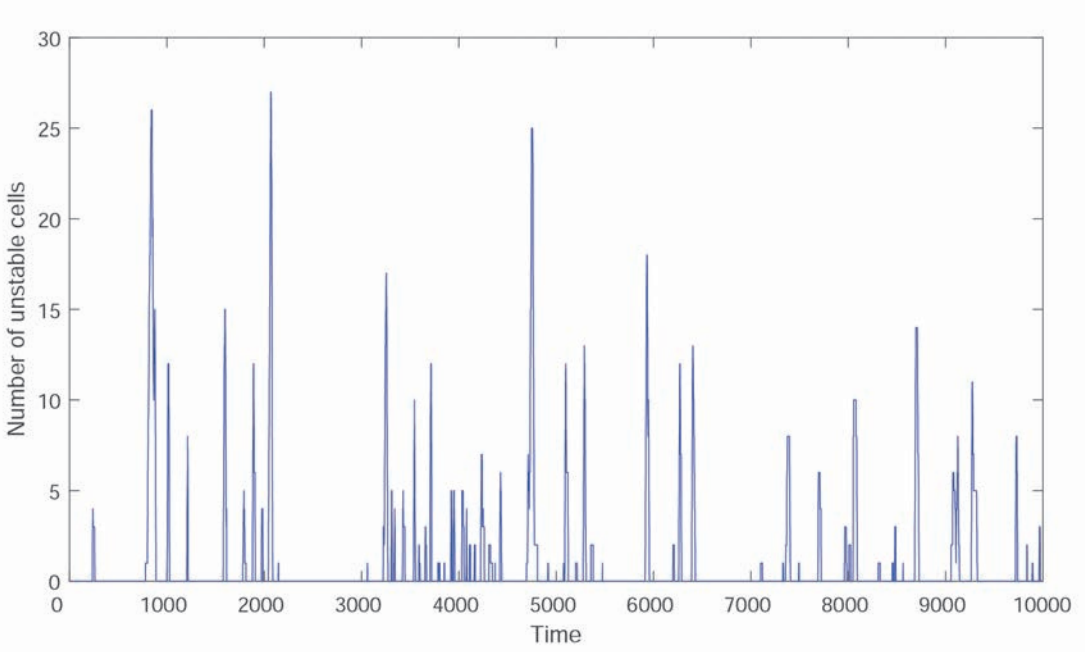

Fig. 5.1. Activity signal example

- **Instantaneous variance of the Shear** σ_{shear}. Shear is one of the basic elements of the extended sandpile. However, shear is different in each cell, and different in each iteration. Due to this, we built a global measure of the importance of the shear and its dynamics by computing its instantaneous variance: σ_{shear}:

$$\sigma_{shear} = \left(\frac{1}{L} \sum_{n=1}^{L} \left(Shear_n - Shear_{average} \right)^2 \right)^{1/2} \tag{5.3}$$

where n indicates the cell number and L is the total number of cells.

$Shear_{average}$ is an average value of shear calculated during a large number of iterations.

- **Instantaneous variance of the gradient** $\sigma_{gradient}$. The reader may recall that the gradient for each cell is the difference in height with the cell to its right. A procedure equal to the one used for shear is used to quantify its global importance and its dynamics. We use the instantaneous variance:. This is,

$$\sigma_{gradient} = \left(\frac{1}{L} \sum_{n=1}^{L} \left(Gradient_n - Gradient_{average} \right)^2 \right)^{1/2} \tag{5.4}$$

Once a sufficient long time series is recorded for these three variables, the transfer entropy analysis is performed for each pair. The result is shown in figure 5.2.

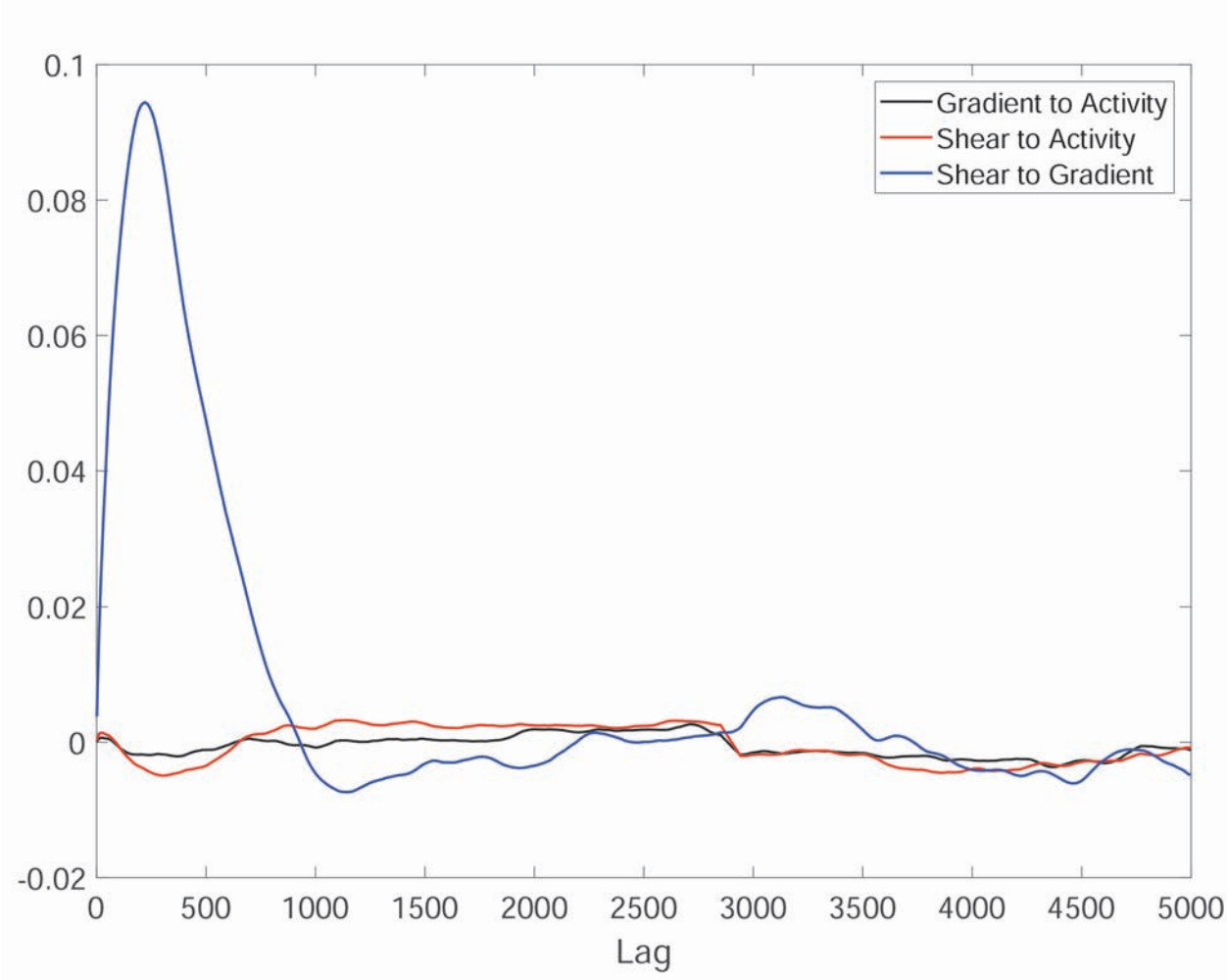

Fig. 5.2. Transfer entropy values for the extended sandpile model with shear

In figure 5.2, a positive value of the transfer entropy means that the transfer takes place in the direction written in the legend; a negative value, that the transfer takes place in the opposite direction.

Figure 5.2 shows the following:

- There is a large positive net transfer entropy value from ”Shear to Gradient” for

short times (500 iterations aprox.). This means that shear is dominant over gradient in the sheared running sandpile. Information on the gradient of the sandpile can be derived by having information on its shear state.

- The influence of shear is much more active over time that the one of the rest of variables. This is due to the fact that once the shear grows, it is very slowly reduced over a long number of iterations as a result of friction forces. During the time that shear is active in the system, it affects importantly the rest of the parameters.

- It is shown that for short times, there is a causal flow from the avalanche activity to shear. Then, on average, the variations in shear are controlled by the amount of avalanches that have taken place. This is a reflection of the fact that, dynamically, shear grows ONLY when avalanches are excited. The transfer is however weaker than in the case of shear to gradient.

- There exists a causal flow from the avalanches activity to the overall gradient of the sandpile, even though this fact is rather weaker. This means that the profile of the sandpile changes only after the avalanches have passed, but their passing is strongly controlled by the value of the shear at the time.

The causal flows in this case are resumed in the following figure, where the strength of the information flow is represented with the arrow thickness:

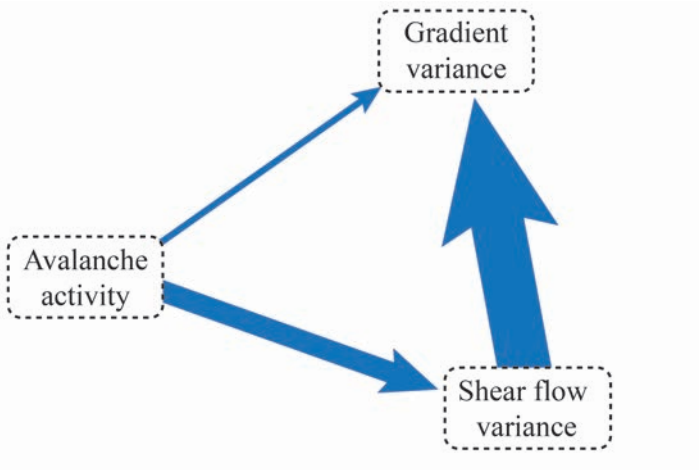

Fig. 5.3. Transfer entropy causal flows in extended running sandpile

The dynamical implications of these results are the following:

- Shear has a predominant effect on the gradient dynamics. Its presence is of greater influence in the short term. Once it appears it rapidly changes the sandpile profile.

- Shear is driven and thus, conditioned, by the activity of avalanches. Therefore, the amount of avalanches that take place in the system seem to be the primary factor

conditioning the transport dynamics, although it does not do it directly but via shear as revealed by the much weaker transfer of entropy to the gradient.

In order to see whether the shear introduced in the extended sandpile in the direction we needed, and the rules implemented in it have changed the dynamics of the running sandpile, transfer entropy from "Gradient to Activity" has been calculated for a running sanpdile with the same parameters but in the absence of shear. The result is shown in figure 5.5.

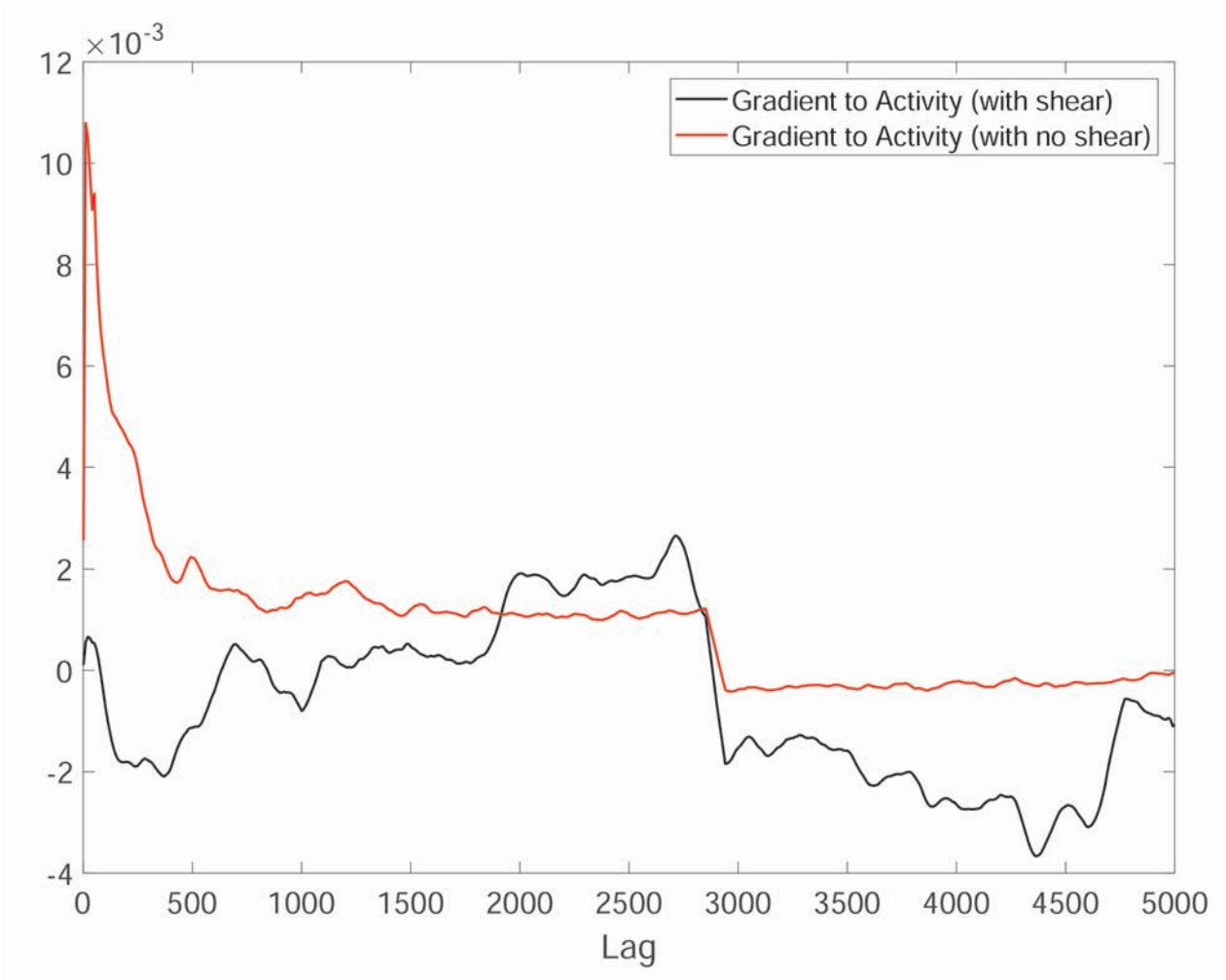

Fig. 5.4. Comparison of Transfer entropy analysis for the extended sandpile model with shear and the running sandpile without shear

It is here evident that the nature of transport has been changed. In the case with shear, the avalanches are responsible for the short term changes in gradient, whereas the opposite relation is found in the case with no shear. This means that the introduction of shear in the model, and the rules created, have changed the essence of transport in the new SOC state. The causal flows have been changed as shown in figure 5.5.

In the case of running sandpile with no shear, the activity of avalanches is a direct consequence of the gradient variance, whereas a more complicated relation between this two

variables that reverts their causality is set when shear acts as a new player in the sandpile model. This may let us state that the created algorithm has been able to incorporate the basic principles of the interaction of shear and turbulence, and may thus constitute a good tool with which the transport dynamics of transport in the H-mode could be studied.

A more extensive study would however require the tuning of the free variables and parameters of the model, so that the relative strength of the couplings between shear, avalanches and profile better represent the situation in the H-mode. This would require a very large number of sandpile runs, since a proper exploration of the parameter space of the extended sandpile should be carried out, which exceeds the objectives of this work.

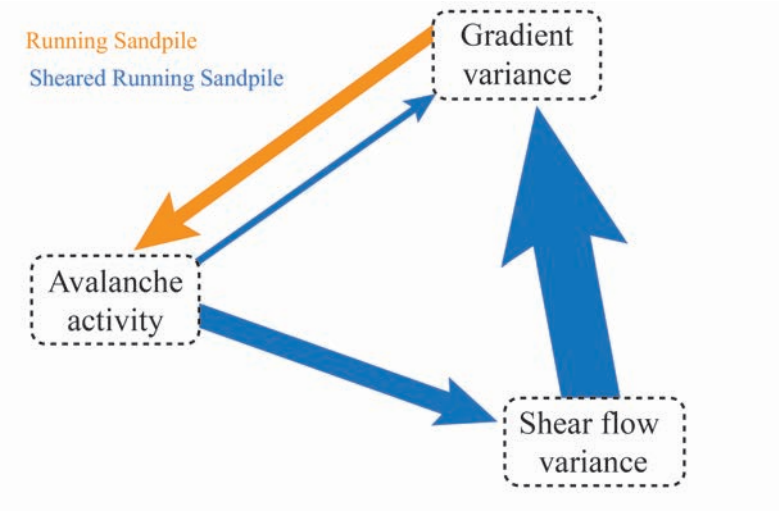

Fig. 5.5. Comparison of Transfer entropy analysis for the extended sandpile model with shear and the running sandpile without shear

6. CONCLUSIONS AND FUTURE WORK

It is then to be concluded that the creation of the extended running sandpile, as described at the beginning of this manuscript, has been successful.

The variables that were introduced and the rules that were created have been shown adequate to recreate and control the essential relationships between the fundamental elements that determine transport dynamics in the presence of a shear flow. Moreover shear became the most important element in the model, something that was intented and sucessfully achieved. This has been proved thanks to the use of transfer entropy, a tool introduced to quantify causal relationships between time series.

The algorithm created, as well as the data selected to be taken out of the simulation runs, provided a correct amount of information to detect these changes in the dynamics of the sandpile.

The present model and research approach have been demonstrated to be able to detect changes in the essential connections between the variables that determine transport. Thus, the procedures followed may be set as a basis to dilucidate the complex relations between shear and turbulence that affect transport dynamics in the H-mode in tokamaks and perceive how are they different from the ones present in L-mode.

For this, additional studies that determine the proper tuning of the variables should be performed in order for the model to closely resemble the dynamics of the H-mode. A numerous amount of simulation runs would be necessary for this purpose and presumably, a computer tool able to process a larger sandpile with a greater number of cells that was beyond the scope and feasibility of the present work.

Once ready, this tool could be extremely useful to undertake studies such as the determination of proper effective transport models based on fractional derivatives, like the ones that have been done with the usual running sandpile during the last two decades [12].

Further speculating, in the case that this model could help anyhow in permiting the understanding of the complexities of H-mode, this could help to clarify the scaling rules of future tokamaks and permit a better prediction on both size and cost of nuclear fusion infrastructures. Who knows if this information will make it more feasible for investors to take an earlier chance on fusion energy industry.

7. SOCIO-ECONOMIC STUDY

7.1. Fusion as the energy source of the future

7.1.1. Socio-Economic impact of Fusion Energy power

It may be said that the fundamental currency of our society nowadays is energy. It powers almost all of our fundamental activities from growing and storing our food to powering our computers.

According to the U.S. Energy Information Administration [20], electricity is mainly obtained from fossil fuels, Nuclear energy and renewable resources. Each of these procedures involve serious drawbacks and consequences either for the environment or for the continuity of their own exploitation.

Several organizations have carried out a number of studies [21] that take into account the environmental costs derived of energy obtained in different ways. Figure 7.1 displays a graph of one of these analysis, revealing that fusion energy would have approximately the same environmental cost as wind energy and way less than fossil resources. However, it must be stated that this data corresponds to studies performed in 2001 and the exact quantification could have been changed in present.

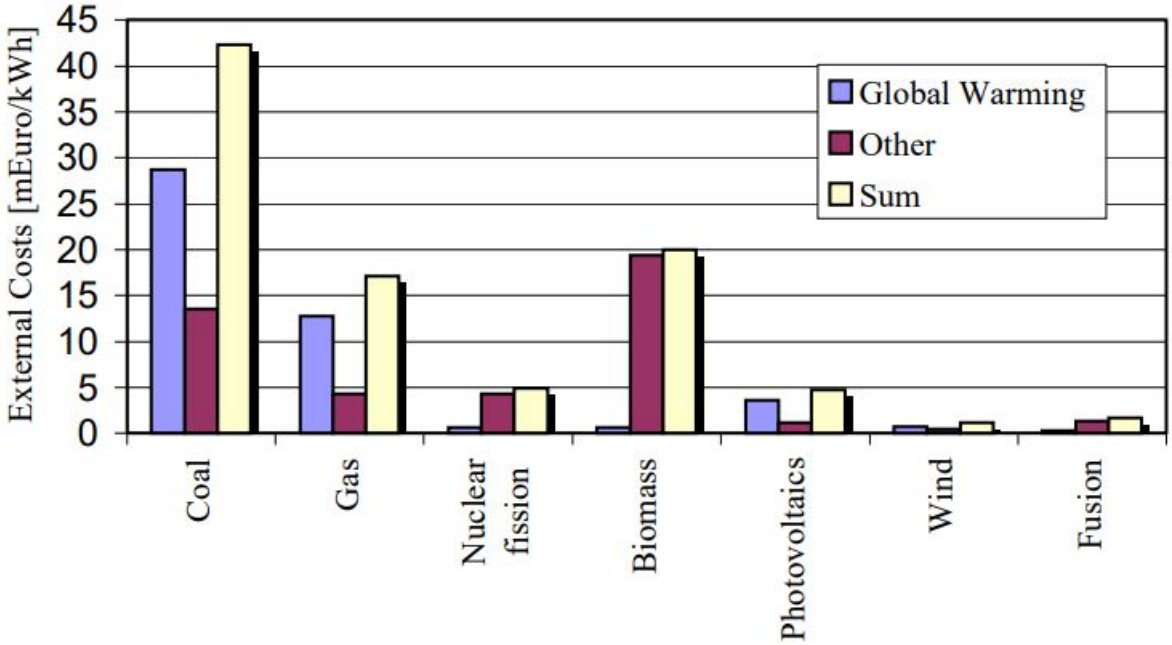

Fig. 7.1. External costs for different electricity sources. The result is split in costs due to emissions of CO_2, sulphur emissions or occupational accidents [Credits to: Ref [21]]

Moreover, studies [22] dealing with the analysis and predictions of costs related to future fusion plants conclude that the costs of electricity produced by fusion would be much less than that obtained through other resources.

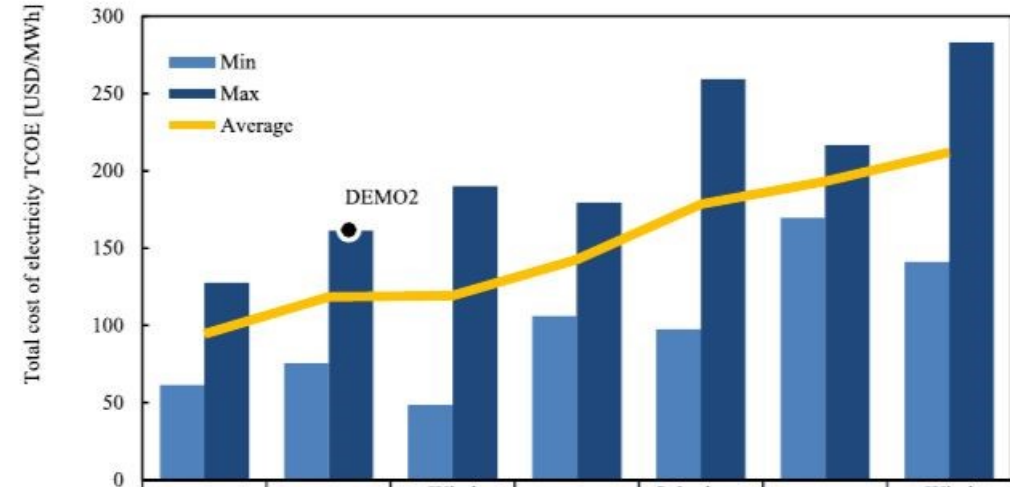

	Nuclear	Fusion	Wind onshore	Natural gas	Solar large PV	Coal	Wind offshore
Min	61	76	49	106	97	170	141
Max	127	161	190	179	259	217	283
Average	94	118	119	143	178	193	212

Fig. 7.2. Total levelized cost of electricity [From *Aproximation of the economy of fusion energy* Ref [22]]. Demo2 is a prototype model based on the most common model for fusion power plant used to retrieve the data in this study.

If these predictions are right, the benefits of fusion energy will be a reality in the future. To reach this, the physics of turbulence inside tokamaks have to be ultimately understood and the reliability of a fusion reactor must be proved first.

7.1.2. Future Nuclear Energy predictions

Nuclear fission is a stable industry today. There exists over 440 nuclear power reactors in operation in 30 different countries [23]. Nuclear fission as a source of energy reached in 2016 its maximum delivery [23] and projects as the Harmony programme [24] from the World Nuclear association are building strategies for producing 25% of global electricity in nuclear reactors by 2050.

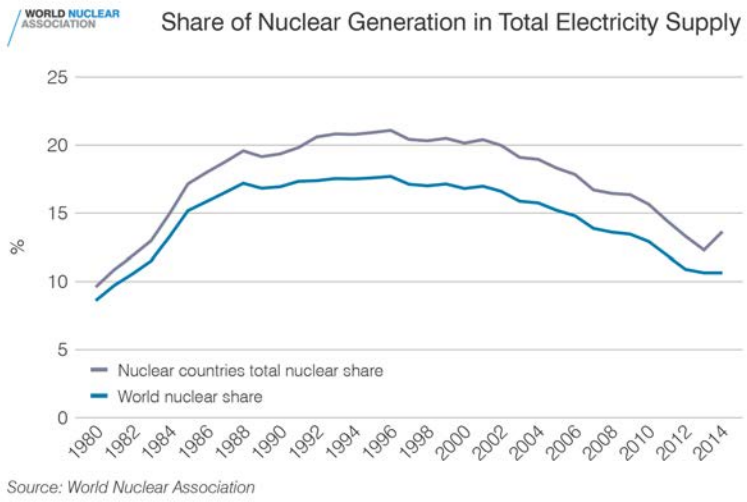

Fig. 7.3. Share of nuclear generation in total electricity supply [From the *World Nuclear Performance Report* Ref [25]]

This data is based on the forecast of a growing demand of both electricity and (fission) nuclear energy reactors. While their vision does not account for a scenario in which fusion energy is a competitor in energy delivery, we can believe that there is a tendency for greater energy demand and reliability on nuclear power in spite of any known drawback to this type of reactors.

Nuclear fusion power would be much safer and profitable in terms of energy than fission nuclear energy. Moreover, as shown in Fig. 7.4 it is observable that a great number of reactors was built before 1990, with less advanced technologies, and will have to be replaced at some point before 2050. What if industrial fusion power was a new player to the energy supply game by then and a technology worth investing in? In the choice of renewing this old plants we could use a new competitor.

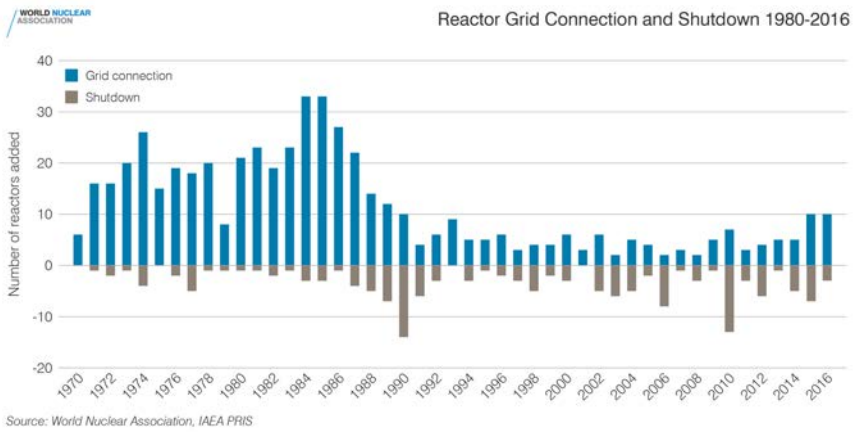

Fig. 7.4. Reactor grid connection and shutdown 1980-2016 [From the *World Nuclear Performance Report* Ref [25]]

7.2. Advantages of fusion over fission

The usual method for obtaining electricity in nuclear reactors nowadays is based on heating water through a chain reaction in the nuclear reactor in which heavy nuclei are fragmented (fission). This heated water powers a steam turbine that generates electricity. This procedure releases a great amount of energy but also entails serious drawbacks that will be addressed in the following lines and compared to its potential competitor: fusion power.

1. The reactants: As it was demonstrated previously, the most reliable fuel to be used in a fusion reactor would be a Deuterium-Tritium mix. Deuterium is very easy to acquire as it can be obtained from water. It is harmless and available in the Earth in virtually unlimited quantities. Tritium however is a bit more difficult to obtain. It can be obtained out of Lithium during fusion reactions. Lithium is expensive but exists in great quantities in the planet. Moreover, tritium is radioactive but its handling in reactors would not imply great danger, fortunately in the case of a leak of tritium due to a fail in the confinement there would only be a few grams of tritium in the vacuum chamber.

   On the other hand, fission reactors usually use heavy elements like uranium enriched 235 or plutonium 239 as fuels.

2. The residues: Nuclear fusion produces no direct nuclear waste. The only byproduct that comes out of the D-T reaction is Helium, which is a non-toxic inert gas and it is naturally stable. The only radioactive waste would come from the activation of the reactor walls by the energetic neutrons produced in the D-T reaction. A careful selection of materials of the walls would however lead to a decay time of hundreds of years, compared with the tens of thousands of fission wastes. These type of residuals could be easily treated on-site with existing technologies.

   Nuclear waste produced by fission is not only radioactive but also contains poisonous elements like plutonium.

3. The reaction: Emulating the energy production of a star in an industrial plant would be less dangerous than it may seem. In the event of failure of the control systems or leakage in the confinement of the very hot plasma, the reaction would simply stop as it would rapidly cool down.

   On the contrary, fission reactions are usually chain reactions that need reactivity control methods and can have catastrophic consequences if uncontrolled.

4. The energy: The Energy density of fusion reactions is many times greater than the one in fission reactions. The energy obtained is also much greater than the one obtained in chemical reactions such as burning of fossil fuels.

7.3. Global socio-economic impact

The industrialization of nuclear (fission) energy was a spin-off to society in the world after World War II. It set a whole new power structure as it meant being more independent to gas or oil imports from other countries.

The industrialization of fusion power generation is a field capable of producing deep socio-political and economical changes in the existing social and political structures. An evidence of this fact is the collaboration without precedents between global powers across the world in the ITER project.

The international consortium of ITER is formed by European Union, Japan, India, the Republic of Korea, the Russian Federation, The United states and the People's Republic of China. All of these countries represent more than half the worlds population and they are committed to a global change.

So even though nowadays scientific efforts are still focused on proving that fusion is feasible at an industrial scale and not on its exploitation, it can already be said the international collaboration on this major potential new technology is already changing the world.

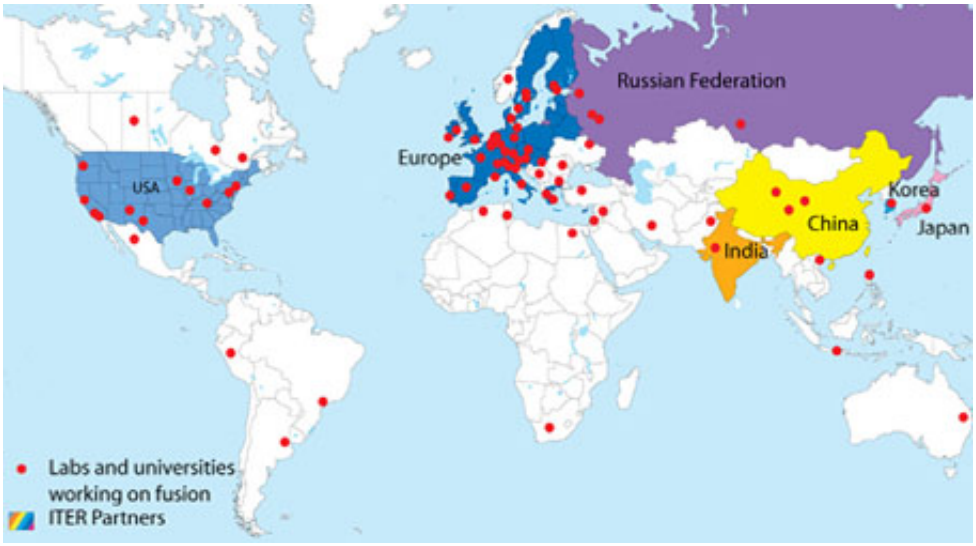

Fig. 7.5. Iter parties [Credits: EFDA European Fusion Development Agreement online site *www.efda.org*]

7.4. Cost of a Tokamak

There is not yet a precise way to estimate the cost of a fusion reactor, since there are still technological decisions to be made. However, most experts would agree that it would certainly lie in the range of several thousand million Euros for a 1-3 GW reactor size. The budget for ITER, that is still an experiment not a reactor, is of 20-40 million Euros. It must be said, however, that research is however significantly more expensive than any

production phase. But ITER's current budget can give an idea of the cost that could be expected for a demo reactor and beyond.

7.5. Budget of the present project

The approximate costs related to the production of this work are detailed in the following tables. They have both been calculated based on the salary for an aerospace engineer in a leadership company and the official salary tables for engineers published in [26]:

TABLE 7.1. LABOUR COSTS

Worker	**Hours worked**	**Price per hour [€\h]**	**Total [€]**
Engineer	*approx* 520 h	14.33	7,461 €
Expert	*approx* 50 h	34.31	1,715 €
Total			**9,176.5 €**

Due to the nature of this project, the main assets used are related to computer and software licensing.

TABLE 7.2. DIRECT COSTS RELATED TO COMPUTER AND SOFTWARE LICENSES

Concept			**Cost [€]**
Computer	Original cost 760 €	33% yearly depreciation	258.4 €
Matlab ®[a]		annual license	800
Office 365 Business ®[b]		annual license	130
Adobe Creative Suite ®[c]		annual license	450
Bibliography access [d]		*approx.*	1,200
Total			**2,838.4 €**

[a] Pricing and licensing Mathworks online site https://es.mathworks.com/campaigns/products
[b] Microsoft office online site https://products.office.com/
[c] Adobe Professional Pricing policy www.adobe.com
[d] Elsevier pricing policy https://www.elsevier.com/about/policies/pricing

Based on research programmes budget performed by other universities [27], the indirect costs due to electricity, transportation, rent of space, fungible material...etc can be approximated as a percentage (44%) of the direct costs so that the final budget would be:

TABLE 7.3. TOTAL BUDGET OF THE PROJECT

Concept	**Cost [€]**
Labour Costs	9,176.5
Computer and software licensing	2,838.4
Indirect costs	5,286.56
Total	**17,301.46 €**

In case this work was ordered by a customer, the charge would include a margin for profit and taxes accounting for **21 %** VAT, so that the final price would be.

TABLE 7.4. PRICE OF THE PROJECT

Concept		**Cost [€]**
Total budget of project		17,301.46
Earnings	10 %	1,730.15
Price withouth taxes		19,031.60
Taxes	21 %	3,996.63
Total Price		**23,0281.24 €**

8. REGULATORY FRAME

As the reader might have noticed, the core of the present project consists on the ideation of a model to help to understand the dynamics of real plasma and its latter implementation and development using computer software.

For this reason, the regulations that are to apply to the present work are limited. These regulations, if any, would be related to the protection of intelectual property and distribution of produced material.

The regulatory framework for these matters in Spain is ruled by the *Código de Propiedad intelectual*, Reference [28], which gives the necessary dispositions to register, deposit and defend intelectual property of created works.

On a separate issue, the present work might leave the way open to improvements that may serve in the future fusion industry, letting its benefits surpass fission energy and letting it become a reliable source of energy.

The agency that is responsible for the regulations that exist at present related to the exploitation and handling of fusion energy is the **IAEA** *The International Atomic Energy Agency*.

Treaties under IAEA are international agreements negotiated by the IAEA member states. The document *"The international legal framework for nuclear security"* Ref.[29], collects international procedures and binding instruments that are aimed to predict, detect and respond to nuclear threats all over the world. In the analysis of Chapter 4. Section 4.2. Ref.[29] of the aforementioned text, some of the purposes for the binding instruments can be distinguished as the following:

1. Physical protection of nuclear material and Nuclear facilities. *INFCIRC/255/Revision 5*.

2. Code of Conduct on the Safety and Security of Radioactive Sources and the Supplementary Guidance on the Import and Export of Radioactive Sources. *GC(47)/RES/7.B*

3. The United Nations Global Counter-Terrorism Strategy *A/RES/60/288* (Non-binding)

This three points are related to the advantages that fusion energy can have over existing fission energy and they have been treated in the previous section. As a conclusion it is to state that the benefits of fusion energy would make these very important points easier to treat.

BIBLIOGRAPHY

[1] R. Sánchez and D. Newman, *A Primer on Complex Systems: With Applications to Astrophysical and Laboratory Plasmas*. Springer, 2018, vol. 943.

[2] R. J. Goldston and P. H. Rutherford, *Introduction to plasma physics*. CRC Press, 1995.

[3] J. D. Lawson, "Some criteria for a power producing thermonuclear reactor," *Proceedings of the Physical Society. Section B*, vol. 70, no. 1, p. 6, 1957.

[4] S. Pfalzner, *An introduction to inertial confinement fusion*. CRC Press, 2006.

[5] C. M. Braams and P. E. Stott, *Nuclear fusion: half a century of magnetic confinement fusion research*. CRC Press, 2002.

[6] M. Wakatani, *Stellarator and heliotron devices*. Oxford University Press on Demand, 1998, vol. 95.

[7] J. Wesson and D. J. Campbell, *Tokamaks*. Oxford University Press, 2011, vol. 149.

[8] B. A. Carreras, "Progress in anomalous transport research in toroidal magnetic confinement devices," *IEEE Transactions on plasma science*, vol. 25, no. 6, pp. 1281–1321, 1997.

[9] R. J. Goldston, "Energy confinement scaling in tokamaks: Some implications of recent experiments with ohmic and strong auxiliary heating," *Plasma Physics and Controlled Fusion*, vol. 26, no. 1A, p. 87, 1984.

[10] F. Wagner, "A quarter-century of h-mode studies," *Plasma Physics and Controlled Fusion*, vol. 49, no. 12B, B1, 2007.

[11] P. Bak, C. Tang, and K. Wiesenfeld, "Self-organized criticality," *Physical review A*, vol. 38, no. 1, p. 364, 1988.

[12] R. Sanchez and D. Newman, "Self-organized criticality and the dynamics of near-marginal turbulent transport in magnetically confined fusion plasmas," *Plasma Physics and Controlled Fusion*, vol. 57, no. 12, p. 123 002, 2015.

[13] T. Hwa and M. Kardar, "Avalanches, hydrodynamics, and discharge events in models of sandpiles," *Physical Review A*, vol. 45, no. 10, p. 7002, 1992.

[14] D. Newman, B. Carreras, P. Diamond, and T. Hahm, "The dynamics of marginality and self-organized criticality as a paradigm for turbulent transport," *Physics of Plasmas*, vol. 3, no. 5, pp. 1858–1866, 1996.

[15] P. Politzer, "Observation of avalanchelike phenomena in a magnetically confined plasma," *Physical review letters*, vol. 84, no. 6, p. 1192, 2000.

[16] P. Terry, "Suppression of turbulence and transport by sheared flow," *Reviews of Modern Physics*, vol. 72, no. 1, p. 109, 2000.

[17] P. Diamond, Y.-M. Liang, B. Carreras, and P. Terry, "Self-regulating shear flow turbulence: A paradigm for the l to h transition," *Physical review letters*, vol. 72, no. 16, p. 2565, 1994.

[18] T. Schreiber, "Measuring information transfer," *Physical review letters*, vol. 85, no. 2, p. 461, 2000.

[19] B. P. van Milligen *et al.*, "The causal relation between turbulent particle flux and density gradient," *Physics of Plasmas*, vol. 23, no. 7, p. 072 307, 2016.

[20] EIA, "Electric power monthly with data for may 2018," U.S. Energy Information Association, Tech. Rep., May 2018.

[21] T. Hamacher, R. Saez, and P. Lako, "Economic and environmental performance of future fusion plants in comparison," Tech. Rep., 2001.

[22] S. Entler, J. Horacek, T. Dlouhy, and V. Dostal, "Approximation of the economy of fusion energy," *Energy*, vol. 152, pp. 489–497, 2018.

[23] IAEA, "International status and prospects for nuclear power 2017," IAEA Atoms for Peace & Development, Tech. Rep., Jul. 2017.

[24] W.N.A., "Harmony, the global nuclear industry's vision for the future of electricity," Wold Nuclear Association, Tech. Rep., 2017.

[25] ——, "World nuclear performance report 2017," Wold Nuclear Association, Tech. Rep., 2017.

[26] Spain, "Boe n. 45," *BOE*, 2018.

[27] *Southern Denmark University*, `https://www.sdu.dk/en/om_sdu/fakulteterne/sundhedsvidenskab/forskning/syddanskforskerstoette/faq/indirect+costs+and+overhead`, Accessed: 2018-09-15.

[28] ——, "Código de propiedad intelectual," *BOE*, 2018.

[29] IAEA, "International legal framework for nuclear security," *IAEA International Law series*, no. 4, p. 23, 2011.

[30] F. Wagner *et al.*, "Regime of improved confinement and high beta in neutral-beam-heated divertor discharges of the asdex tokamak," *Physical Review Letters*, vol. 49, no. 19, p. 1408, 1982.

[31] Y. Xu, "A general comparison between tokamak and stellarator plasmas," *Matter and Radiation at Extremes*, vol. 1, no. 4, pp. 192–200, 2016.

[32] R. Arnoux, *Turbulent behaviour under radar scrutiny*, www.iter.org, Ed., [Online], Jul. 2010.

[33] ——, *How fritz wagner discovered the h mode*, www.iter.org, Ed., [Online], Jun. 2009.

[34] S. Kayne and R.J.Goldston, "Global energy confinement scaling for neutral-beam-heated tokamaks," *IAEA Nuclear Fusion*, vol. 25, no. 65, 1985.

[35] R. Sánchez, D. Newman, and B. Carreras, "Mixed soc diffusive dynamics as a paradigm for transport in fusion devices," *Nuclear Fusion*, vol. 41, no. 3, p. 247, 2001.

[36] V. Kenkre, E. Montroll, and M. Shlesinger, "Generalized master equations for continuous-time random walks," *Journal of Statistical Physics*, vol. 9, no. 1, pp. 45–50, 1973.

[37] N. Wiener, "The theory of prediction," *Modern mathematics for engineers*, 1956.

[38] H. E. Hurst, "Long-term storage capacity of reservoirs," *Trans. Amer. Soc. Civil Eng.*, vol. 116, pp. 770–799, 1951.

[39] K. Gentle *et al.*, "An experimental counter-example to the local transport paradigm," *Physics of Plasmas*, vol. 2, no. 6, pp. 2292–2298, 1995.

[40] S.-K. Ma, *Modern theory of critical phenomena*. Routledge, 2018.

[41] J. Sheffield and A. Gibson, "Cost scaling of tokamaks," *Nuclear Fusion*, vol. 15, no. 4, p. 677, 1975.